


Nonlinear optical responses in nodal line semimetals

Omid Tavakol and Yong Baek Kim

Department of Physics, University of Toronto, Toronto, Ontario, Canada M5S 1A7

 (Received 4 April 2022; revised 27 October 2022; accepted 14 December 2022; published 10 January 2023)

Nonlinear optical responses, such as shift current and second-harmonic generation (SHG), of topological semimetals have been subjects of great interest because the momentum-space topological structures near Weyl or Dirac points lead to unusually large responses. This is especially important for technological applications as the shift current and SHG are often used for solar cell and frequency-changing applications for lasers, respectively. We demonstrate that nodal line semimetals can offer even larger responses at low frequencies. For example, we show that a large SHG response arises at finite doping when an external dc electric field is applied to break the inversion symmetry of an otherwise inversion-symmetric model of a nodal line semimetal. Furthermore, we introduce a model with intrinsically broken inversion symmetry, where both the shift current and SHG are singular in a range of parameters.

DOI: [10.1103/PhysRevB.107.035114](https://doi.org/10.1103/PhysRevB.107.035114)

I. INTRODUCTION

Nonlinear optical responses of quantum materials offer a deeper understanding of many-body excitation spectra [1], which may help us build more useful optical devices [2]. Recent studies show that the bulk photovoltaic effect or the shift current, which is a nonlinear optical response producing a net photocurrent in noncentrosymmetric materials [3–7], is a promising substitute for conventional solar cells with *pn* junctions [8]. Furthermore, second-harmonic generation (SHG) is another second-order nonlinear optical response, where the material absorbs a light with frequency ω and produces a light with doubled frequency 2ω [9–13]. The symmetry structure of the SHG tensor provides important information about the subtle broken symmetries in materials [14,15], which may not be obvious in linear response probes. Although the basic principles of these nonlinear responses are well understood [9,16,17], it is highly valuable to investigate materials that may provide strong nonlinear optical responses.

Recently, it has been shown that topological semimetals such as Weyl semimetals [18], where the valence and conduction bands cross each other in momentum space at a discrete set of points, can produce strong nonlinear optical responses [19–25]. These responses are intimately related to the topology of the wave function near the band-crossing points, known as Weyl points [26–29]. For example, a strong nonlinear optical response was observed in a Weyl semimetal with broken inversion symmetry, TaAs [2,21,30,31].

In this paper, we investigate nonlinear optical responses in a class of topological nodal line semimetals (NLSMs) [32–34]. The crossing points between conduction and valence bands form a closed loop in the momentum space, and upon doping, a Fermi surface with the topology of a torus arises as shown in Fig. 1. There exist a number of materials that show NLSM behavior such as HgCr₂Se₄ [35], Cu₃PdN [36], Cu₃ZnN [37], Ca₃P₂ [38], ZrSiS [39], and SrIO₃ [40]. The

NLSM exhibits various exotic properties due to the nontrivial structure of the Fermi surface [41,42], which includes a parity anomaly [43] and a giant nonlinear response in the presence of magnetic fields [44].

The most important quantities that can affect nonlinear optical conductivity are energy dispersion and the topology of the Bloch wave function. In this paper, we consider a class of NLSM models with different dispersions and study the behaviors of the shift current and SHG. Since these nonlinear responses arise when the inversion symmetry is broken, we consider the systems where the inversion symmetry is broken either intrinsically or via an external electric field. We first consider the NLSM where the inversion symmetry is broken by an external electric field. It is found that SHG in the NLSM can have a more singular response in comparison to the Weyl semimetal, i.e., $\sigma_{\text{SHG}}^{\text{NLSM}} \sim \sigma_{\text{SHG}}^{\text{Weyl}}(\frac{vk_0}{\mu})$ in the low-doping limit $\mu \rightarrow 0$ (vk_0 is an energy scale associated with the NLSM). Furthermore, considering the NLSM systems with intrinsically broken inversion symmetry, we show that a certain class of NLSMs can have stronger shift current (and similarly SHG) responses, $\sigma_{\text{shift,NLSM}}^{\text{zzz}}(0; \omega, -\omega) \propto (e^3/\hbar^2)\omega^{-3/2}$, in comparison to the case of Weyl semimetals $\sigma_{\text{shift,Weyl}}^{\text{zzz}}(0; \omega, -\omega) \propto (e^3/\hbar^2)\omega^{-1}$ in the low-frequency limit. We explain below how these singular behaviors arise from the peculiar structure of the Fermi surface and the Berry curvature of the wave function in NLSMs.

The rest of this paper is organized as follows. In Sec. II, we discuss the nonlinear optical response functions in different gauge choices. In particular, the relations between the expressions of shift current and SHG with different gauge choices are discussed. In Sec. III, we consider a NLSM where the inversion is broken by an external dc electric field. We show the behavior of SHG in this system. In Sec. IV, we introduce two classes of NLSM systems with intrinsically broken inversion symmetry. We study both the shift current

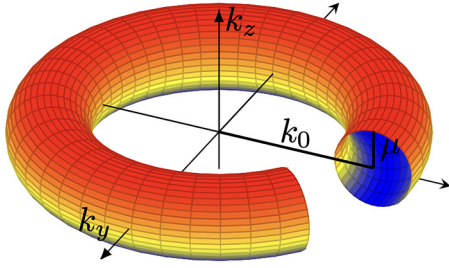


FIG. 1. The Fermi surface of a NLSM. The radius of the torus is considered to be k_0 , and $k_0 > \mu$, where μ is the chemical potential.

and SHG and present their behaviors. In Sec. V, we discuss the implications of our results.

II. NONLINEAR OPTICAL RESPONSES IN LENGTH AND VELOCITY GAUGES

A. Length and velocity gauges

We first discuss two gauge choices that are commonly used to calculate nonlinear responses. These two gauges are known as the velocity gauge and the length gauge. The advantage of making these two gauge choices in nonlinear response calculations is that the structure of the resulting Hamiltonian is linear in the gauge field and it simplifies the calculation of response functions. In the rest of the paper, we use the length gauge to calculate the shift current, and we use both the velocity gauge and the length gauge to calculate SHG.

To introduce these two gauges, let us consider a general dispersion $H_0 = \varepsilon(\mathbf{p})$ and a Hamiltonian $H(\mathbf{p}, \mathbf{r}) = H_0 + V_{\text{int}}(\mathbf{r})$. In the presence of an external gauge field, one can use the minimal substitution $\mathbf{p} \rightarrow \mathbf{p} - e\mathbf{A}$. Then the Hamiltonian up to the second order in the gauge field can be written in the following form:

$$H = \varepsilon(\mathbf{p}) - e\nabla_p \varepsilon(\mathbf{p}) \cdot \mathbf{A} + \frac{e^2}{2} \nabla_p^2 \varepsilon(\mathbf{p}) (\mathbf{A} \cdot \mathbf{A}) + O(\mathbf{A}^3) - e\phi, \quad (1)$$

where \mathbf{A} and ϕ are vector and scalar potentials of the electromagnetic field. In the absence of any static source, we can assume that $\phi(r, t) = 0$, and also in the dipole approximation, we can take the vector potential to be independent of position $\mathbf{A}(r, t) = \mathbf{A}(t)$. In finding the second-order response, the quadratic term in the gauge field can make the calculation much more difficult. As a result, it would be more efficient to cancel this term by fixing a gauge. The first gauge that can be used is the length gauge. The freedom of gauge transformation can be written as follows:

$$\begin{aligned} \mathbf{A} &\rightarrow \mathbf{A}' = \mathbf{A} + \nabla \Lambda, \\ \phi &\rightarrow \phi' = \phi - \partial_t \Lambda, \\ \psi &\rightarrow \psi' = e^{-ie\Lambda/\hbar} \psi, \end{aligned} \quad (2)$$

where ψ is the matter field or wave function.

By choosing $\Lambda = -\mathbf{A}(t) \cdot \mathbf{r}$, which is the length gauge choice, we get $\mathbf{A}' = 0$ and $\phi' = \partial_t \mathbf{A}(t) \cdot \mathbf{r} = -\mathbf{E}(t) \cdot \mathbf{r}$. By making the vector potential vanish, the only term contributing to the Hamiltonian is the scalar potential. Thus the Hamiltonian in the presence of an external electric field in the length

gauge can be written in the following form:

$$H_L(\mathbf{p}, \mathbf{r}) = \varepsilon(\mathbf{p}) + e\mathbf{E}(t) \cdot \mathbf{r}, \quad (3)$$

where the subscript L denotes that the Hamiltonian is written in the length gauge. $\mathbf{E}(t)$ is the electric field, and the $e\mathbf{E}(t) \cdot \mathbf{r}$ term can be interpreted as an interaction between the electric field and the polarization $\hat{\mathbf{P}}_{\text{tot}} = -e\hat{\mathbf{r}}$.

In systems with multiband structure, there exist two kinds of polarizations due to the interband and intraband interactions, which we denote as \mathbf{P}_e and \mathbf{P}_i , respectively. The second quantized forms of the polarizations can be written as follows:

$$\hat{\mathbf{P}}_e = e \int [dk] \sum_{nm} \mathbf{r}_{nm} a_n^\dagger(k) a_m(k), \quad (4)$$

$$\hat{\mathbf{P}}_i = e \int [dk] \sum_n (a_n^\dagger(k) \partial_{\mathbf{k}} a_n(k) - i\xi_{nm} a_n^\dagger(k) a_n(k)), \quad (5)$$

where $[dk] = \frac{d^3k}{(2\pi)^3}$. Here, a^\dagger and a are fermionic creation and annihilation operators. ξ_{nm} is the Berry connection of the n th band, and \mathbf{r}_{nm} is the expectation value of the position operator between n and m states, $\langle n | \mathbf{r} | m \rangle$, which can be written in the following form:

$$\begin{aligned} \xi_{nm} &= iu_n(k)^* \partial_{\mathbf{k}} u_m(k), \\ \mathbf{r}_{nm} &= \xi_{nm} \quad \text{when } n \neq m, \end{aligned} \quad (6)$$

where $u_n(k)$ is the periodic part of the Bloch wave function.

On the other hand, for the velocity gauge, we can choose $\Lambda = -\nabla_p^2 \varepsilon(p) \frac{e}{2m} \int_{-\infty}^t \mathbf{A}(t') \cdot \mathbf{A}(t') dt'$. Thus we find $\mathbf{A}' = \mathbf{A}(t)$ and $\phi' = \nabla_p^2 \varepsilon(p) \frac{e}{2m} \mathbf{A}(t) \cdot \mathbf{A}(t)$. Then, in this gauge, the scalar potential cancels the nonlinear gauge field term, and the Hamiltonian turns out to be

$$H_V = \varepsilon(p) + e\mathbf{A}(t) \cdot \nabla_p \varepsilon(p), \quad (7)$$

where the subscript V denotes that the Hamiltonian is written in the velocity gauge. Note that the Hamiltonians in both gauge choices are linear in the external gauge field, making the calculation easier.

We note that, at first glance, the calculation of the nonlinear response seems simpler in the velocity gauge compared with the length gauge since there is no spatial dependence in the Hamiltonian. This means that one can find the system's response for each lattice momentum individually. However, it was shown that the velocity gauge can give rise to unphysical divergences at low frequencies [45]. This problem was addressed by Aversa and Sipe [6]; they calculated the diverging coefficients and expressed them in terms of sum rules. They have further shown that, in a full band calculation when all the sum rules are satisfied, the diverging coefficients sum to zero and the result is gauge invariant. However, these sum rules can be easily violated by truncating bands, which can give rise to nonphysical divergences in the velocity gauge. On the other hand, determining the nonlinear responses in the length gauge seems more reliable in the finite-band approximation since there is no evidence of these divergences in the length gauge calculation of nonlinear responses. This means that the divergence of a quantity computed in the velocity gauge may be physical or unphysical depending on the situation. To distinguish these two cases, the calculation must also be done in the length gauge, which does not suffer from unphysical

divergences. Such a situation may apply to our calculation of SHG in the velocity gauge in Sec. III. Thus, in Appendix E, we discuss the calculation of SHG in the length gauge mainly to demonstrate that the low-frequency singularity responsible for the large SHG is the same in the velocity gauge and in the length gauge.

B. Shift current and second-harmonic generation

In the presence of an electric field \mathbf{E} , the response of the system can be written in terms of an expansion of the current, \mathbf{J} , as a function of the electric field,

$$J^a(\omega) = \sigma^{ab}(\omega)E^b(\omega) + \sigma^{abc}(\omega; \omega_1, \omega_2)E^b(\omega_1)E^c(\omega_2) + \dots, \quad (8)$$

where $a, b, c \in \{x, y, z\}$, $\omega = \omega_1 + \omega_2$, and $E(\omega_1)$ is the Fourier component of the time-dependent electric field. In this manner, $\sigma^{ab}(\omega)$ is the linear response and $\sigma^{abc}(\omega; \omega_1, \omega_2)$ is the second-order nonlinear response to the incident light. There are a number of nonlinear optical processes that can occur in the presence of an electric field, which include SHG, sum and difference frequency generation, and shift current, which are also known as bulk photovoltaic effects (BPVEs). These second-order responses can be observed in systems with broken inversion symmetry. In this paper, we only focus on the SHG and shift current.

1. Shift current

In systems with broken inversion symmetry, the separation of centers of charge in valence and conduction bands can produce the net dc current, known as the shift current [16]. In the length gauge formulation, if the light is polarized in the b direction, the shift current can be written in the following form [5,6,9]:

$$\begin{aligned} \sigma_{\text{shift}}^{\text{abb}}(0; \omega, -\omega) \\ = \frac{\pi e^3}{\hbar^2} \sum_{nm} \int_{\text{BZ}} [dk] |r_{nm}^b(k)|^2 R_{nmb}^a(k) f_{nm} \delta(\omega_{nm} - \omega), \end{aligned} \quad (9)$$

where the sum is over the band index and BZ refers to the Brillouin zone. Here, $a, b \in \{x, y, z\}$ are spatial coordinates, and $f_{nm} = f(\epsilon_n) - f(\epsilon_m)$, where $f(\epsilon)$ is the Fermi distribution function. Note that $\epsilon_n = \hbar\omega_n$ is the eigenvalue of the Bloch Hamiltonian $H(k)$ and $\omega_{nm} = \omega_n - \omega_m$. Moreover, $f_{nm}|r_{nm}^b(k)|^2$ is related to the transition intensity, and $R_{nmb}^a(k)$ denotes the separation of centers of charge (in the valence and conduction bands) in the real space, which is known as the shift vector

$$R_{nmb}^a(k) = -\frac{\partial \phi_{nm}^b}{\partial k_a} + \xi_{nm}^a - \xi_{mm}^a. \quad (10)$$

Here, $\phi_{nm}^b = \text{Im}[\ln(r_{nm}^b)]$ is the phase of the matrix element of the position operator.

2. Second-harmonic generation

In the SHG process, systems with broken inversion symmetry can absorb a light with frequency ω and produce a light with doubled frequency 2ω . The corresponding nonlinear current can be written as $J^a(2\omega) = \sigma^{abc}(2\omega; \omega, \omega)E^b(\omega)E^c(\omega)$. Here, the SHG response tensor in the velocity gauge can be

defined as follows [10,30]:

$$\sigma_{\text{SHG}}^{abc}(\omega) = \sigma_{2p,1}^{abc}(\omega) + \sigma_{2p,\text{II}}^{abc}(\omega) + \sigma_{1p,1}^{abc}(\omega) + \sigma_{1p,\text{II}}^{abc}(\omega), \quad (11)$$

where

$$\sigma_{2p,1}^{abc}(\omega) = \sum_{nm} \frac{e^3}{2\hbar^2 \omega^2} \int [dk] v_{mn}^a w_{nm}^{bc} f_{mn} R_\gamma(2\omega - \omega_{nm}), \quad (12)$$

$$\begin{aligned} \sigma_{2p,\text{II}}^{abc}(\omega) = \sum_{nmp} \frac{e^3}{2\hbar^2 \omega^2} \int [dk] \frac{2v_{mn}^a [v_{np}^b v_{pm}^c]_+}{\omega_{mp} + \omega_{np}} \\ \times f_{mn} R_\gamma(2\omega - \omega_{nm}), \end{aligned} \quad (13)$$

$$\begin{aligned} \sigma_{1p,1}^{abc}(\omega) = \sum_{nm} \frac{e^3}{2\hbar^2 \omega^2} \int [dk] (w_{mn}^{ab} v_{nm}^c + w_{mn}^{ac} v_{nm}^b) \\ \times f_{mn} R_\gamma(\omega - \omega_{nm}), \end{aligned} \quad (14)$$

$$\begin{aligned} \sigma_{1p,\text{II}}^{abc}(\omega) = \sum_{nmp} \frac{e^3}{2\hbar^2 \omega^2} \int [dk] \frac{v_{mn}^a [v_{np}^b v_{pm}^c]_+}{\omega_{pm} + \omega_{pn}} \\ \times (f_{mp} R_\gamma(\omega - \omega_{pm}) - f_{np} R_\gamma(\omega - \omega_{np})). \end{aligned} \quad (15)$$

Here, $w^{ab} = (1/\hbar)\partial_{k_a}\partial_{k_b}H$, $[v_{np}^b v_{pm}^c]_+ = v_{np}^b v_{pm}^c + v_{np}^c v_{pm}^b$, and $R_\gamma(x) = 1/(x - i\gamma)$, where γ is related to the decay rate. SHG consists of four different processes, Eqs. (12)–(15). The first two equations, Eqs. (12) and (13), which are denoted by index $2p$, show the contributions of two-photon resonance. On the other hand, Eqs. (14) and (15), denoted by $1p$, show the contributions of one-photon resonance.

III. NODAL LINE SEMIMETAL WITH INVERSION-BREAKING EXTERNAL ELECTRIC FIELD

In this section, we start with an inversion-symmetric model for nodal line semimetals. Then, in order to find a finite SHG response, we break the inversion symmetry by applying an external electric field. We find the analytic expression for SHG in this case.

Let us consider the following Hamiltonian [46]:

$$H(k) = v(\sqrt{k_x^2 + k_y^2} - k_0)\tau_x + vk_z\tau_z, \quad (16)$$

where τ_A are the Pauli matrices acting on the orbital space, where $A \in \{x, y, z\}$. Here, k_0 is the radius of the nodal line in the momentum space. The location of the zero-energy nodal line spectrum is given by $\sqrt{k_x^2 + k_y^2} = k_0$ and $k_z = 0$. This Hamiltonian preserves both time-reversal and inversion symmetry as it commutes with the parity operator $\mathcal{P} = \tau_x \otimes (k \rightarrow -k)$ and the time-reversal operator $T = K \otimes (k \rightarrow -k)$, where K is the complex-conjugate operator.

Now we introduce an external electric field to break the inversion symmetry. In systems with inversion symmetry, the second-order nonlinear response would vanish, and only odd responses would contribute to the current density. However, in the presence of an external dc electric field, the distribution function of electrons breaks the inversion symmetry, and this gives rise to a second-order nonlinear response such as SHG.

In the presence of an external dc electric field, we can find the distribution function using the Boltzmann equation by

introducing a relaxation time τ ,

$$-\frac{e}{\hbar} \mathbf{E} \cdot \partial_{\mathbf{k}} f = -\frac{\delta f}{\tau}. \quad (17)$$

By solving the Boltzmann equation, one can obtain the distribution function for the n th band

$$f_n = f_n^{(0)} + \frac{e\tau}{\hbar} \mathbf{E} \cdot \partial_{\mathbf{k}} f_n^{(0)} + \frac{e\tau}{\hbar} E^a E^b \partial_{k_a} f_n^{(0)} \partial_{k_b} f_n^{(0)}, \quad (18)$$

where $f_n^{(0)}$ is the equilibrium distribution function. The important contribution is the linear term in the electric field, which breaks the inversion and gives rise to the SHG.

Let us consider a dc electric field in the z direction. In our model, in the low-frequency limit, $\sigma_{2p,1}^{abc}$ and $\sigma_{1p,1}^{abc}$ vanish. Note that these two contributions also vanish in semimetals with a linear dispersion, such as Weyl semimetals [16]. The reason why these contributions vanish in Weyl semimetals is that the second derivative of the Hamiltonian, which enters in $\sigma_{2p,1}^{abc}$ and $\sigma_{1p,1}^{abc}$, is zero. However, in our model, these terms do not vanish explicitly, but the integral over the Fermi surface vanishes because they are odd functions of momentum. The only important remaining terms are $\sigma_{2p,\text{II}}^{abc}$ and $\sigma_{1p,\text{II}}^{abc}$ in Eqs. (13) and (15), respectively. Both of these terms scale similarly with respect to frequency, which is explained in the analytic expression of SHG in Appendix C.

In the case of $\mu < vk_0$, where μ is the chemical potential, we have the following form for SHG:

$$\sigma_{\text{SHG}}^{abc}(2\omega; \omega, \omega) = \sigma_{2p,\text{II}}^{abc}(2\omega; \omega, \omega) + \sigma_{1p,\text{II}}^{abc}(2\omega; \omega, \omega), \quad (19)$$

where

$$\sigma_{2p,\text{II}}^{abc}(2\omega; \omega, \omega) = \frac{e^4 v^2 E_z k_0 \tau}{\hbar^3 \mu^2} R_\gamma(2\omega - 2\mu) C_{2p,\text{II}}^{abc}, \quad (20)$$

$$\sigma_{1p,\text{II}}^{abc}(2\omega; \omega, \omega) = \frac{e^4 v^2 E_z k_0 \tau}{\hbar^3 \mu^2} R_\gamma(\omega - 2\mu) C_{1p,\text{II}}^{abc}. \quad (21)$$

Here, $C_{1p,\text{II}}^{abc}$ and $C_{2p,\text{II}}^{abc}$ are numerical coefficients shown in Table III in Appendix C, and $R_\gamma(\omega - 2\mu) = \frac{1}{\hbar\omega - 2\mu - i\gamma}$. We assume that γ is sufficiently small so that the resonant factor $R_\gamma(x)$ behaves like $\delta(x)$. Thus we used the approximations $\omega \sim 2\mu$ and $\omega \sim \mu$ for the one-photon and two-photon resonances, respectively.

In the limit $\mu \ll vk_0$, the SHG is singular as

$$\sigma_{\text{SHG}}^{nod} \sim k_0/\mu^2, \quad (22)$$

which is more divergent in comparison to the case of a Weyl semimetal, $\sigma_{\text{SHG}}^{\text{Weyl}} \sim 1/\mu$. On the other hand, in the opposite limit, $vk_0 \ll \mu$, we obtain

$$\sigma_{\text{SHG}}^{nod} \sim 1/\mu + k_0/\mu^2 + O((k_0/\mu)^2). \quad (23)$$

Note that in the limit $k_0 \rightarrow 0$, this result reduces to the same behavior as in a Weyl semimetal.

IV. NODAL LINE SEMIMETAL WITH INTRINSICALLY BROKEN INVERSION SYMMETRY

In this section, we introduce two sets of Hamiltonians (models 1 and 2) for a NLSM with intrinsically broken inversion symmetry. We also consider tunable dispersions in these models, which lead to different behaviors in the density

of states. For each model, we compute the shift current and SHG for different dispersion relations, and we show that some choice of dispersion can enhance the shift current response.

A. Two models

Let us first consider the following 2×2 Hamiltonian, which we call model 1.

$$H(k) = t_x (\sqrt{k_x^2 + k_y^2} - k_0)^a \tau_x + v_y k_z \tau_y + t_z k_z^b \tau_z, \quad (24)$$

where τ_A are Pauli matrices acting on the orbital space, where $A \in \{x, y, z\}$. k_0 is the radius of the nodal line in momentum space. The location of the zero-energy nodal line is given by $\sqrt{k_x^2 + k_y^2} = k_0$ and $k_z = 0$.

There is another class of Hamiltonian that can capture the features of nodal line semimetals but with different scaling with respect to x , y , and z directions [43,44,47–49]. This effective Hamiltonian, which we call model 2, can be written in the following form:

$$\tilde{H} = \tilde{t}_x (k_x^2 + k_y^2 - k_0^2)^a \tau_x + v_y k_z \tau_y + t_z k_z^b \tau_z. \quad (25)$$

In both models, the Hamiltonian can break inversion symmetry or time-reversal symmetry depending on the exponent b . This can be determined by considering the commutation relation between the Hamiltonian and the parity operator $\mathcal{P} = \tau_x \otimes (k \rightarrow -k)$ and between the Hamiltonian and the time-reversal operator $T = K \otimes (k \rightarrow -k)$, where K is the complex-conjugate operator. In this model, the τ_z term breaks the inversion when b is an even integer (but preserves time-reversal symmetry). Note that, as long as $b > 1$, the τ_z term can be regarded as a small perturbation in the low-frequency limit. We investigate the behavior of the shift current depending on the choice of a and b .

B. Shift conductivity

One of the important factors determining the scaling behavior of the shift current is the joint density of states, $\rho(\epsilon)$. This, as well as the shift vector and transition intensity, determine the scaling behavior of the shift conductivity in the low-frequency limit. In the following, we examine the contribution of each of these three quantities to the shift current in models 1 and 2, respectively. The joint density of states for these two models can be written as follows. The quantity represented by the variables with the tilde sign is for model 2.

$$\begin{aligned} \rho(\omega) &= \frac{1}{V} \int [dk] \delta(\omega - \omega_{cv}(k)) \\ &= 2\pi \frac{4k_0 \sqrt{\pi}}{v_y} \left(\frac{\omega}{t_x} \right)^{\frac{1}{a}} \frac{\Gamma(1 + \frac{1}{2a})}{\Gamma(\frac{1+a}{2a})}, \end{aligned} \quad (26)$$

$$\begin{aligned} \tilde{\rho}(\omega) &= \frac{1}{V} \int [dk] \delta(\omega - \tilde{\omega}_{cv}(k)) \\ &= 2\pi \frac{\sqrt{\pi}}{av_y} \left(\frac{\omega}{\tilde{t}_x} \right)^{\frac{1}{a}} \frac{\Gamma(\frac{1}{2a})}{\Gamma(\frac{1+a}{2a})}. \end{aligned} \quad (27)$$

Here, $\hbar\omega_{cv} = \epsilon_c - \epsilon_v$, $\hbar\tilde{\omega}_{cv} = \tilde{\epsilon}_c - \tilde{\epsilon}_v$ and c, v represent the conduction and valence bands. For both models, the scaling of the density of states as a function of energy is the same.

However, in model 1, the presence of a finite radius k_0 is crucial to find a nonzero density of states, which is not the case for model 2.

Let us first consider model 1. To find the relation between the joint density of states and shift conductivity in Eq. (9), we change the integral variable from lattice momentum to ϵ and Ω , which are the energy and the solid angle in momentum space, respectively. Then we can find the following form for the shift conductivity:

$$\sigma_{\text{shift}}^{ijj}(\omega) = \int d\Omega d\epsilon I^{ijj}(\theta, \epsilon) f_{cv}(\epsilon) \delta(\omega_{cv} - \omega),$$

where

$$I^{ijj}(\theta, \epsilon) = |\det J| |r_{cv}^j(\epsilon, \theta)|^2 R_{cv,j}^i(\epsilon, \theta). \quad (28)$$

Here, $f_{cv}(\epsilon) = f(\epsilon_c) - f(\epsilon_v)$, $|\det J|$ is the determinant of the Jacobian matrix, and $i, j \in \{x, y, z\}$. The exact expression of the Jacobian determinant is discussed in Appendix B and shown in Eq. (B5). It can be schematically written as $|\det J|(\epsilon, \theta) = k_0 \epsilon^{1/a} u_a(\theta) + \epsilon^{2/a} g_a(\theta)$. Here, u_a and g_a are functions of θ and a . The contribution of the first term corresponds to the joint density of states for model 1, shown in Eq. (26). This can be seen from $\int d\Omega |\det J|(\epsilon, \theta) \propto \rho(\epsilon)$ due to $\int d\Omega g_a(\theta) = 0$. Thus we can write the determinant of the Jacobian matrix in terms of the joint density function, $|\det J|(\epsilon, \theta) = \rho(\epsilon) h_a(\theta) + \epsilon^{2/a} g_a(\theta)$. Here, $h_a(\theta)$ and $u_a(\theta)$ differ only by a multiplicative constant. For the scaling behavior of the shift conductivity, the other two important factors are the transition intensity, which is proportional to the interband element of the position operator $|r_{nm}^j|^2$, and the shift vector in Eq. (10).

To investigate the contribution of each term, we need to choose a direction. Because of the symmetry of the Hamiltonians, the x and y directions behave similarly, so let us only consider the zzz and zxx directions. Let us first consider the zzz direction. In our two-band Hamiltonian models, in the low-frequency limit, we find that the interband element of the position operator scales as $|r_{cv}^z(\epsilon, \theta)|^2 = \epsilon^{-2} h^{r,z}(\theta)$. Here, $h^{r,z}(\theta)$ is an angular part of the $|r_{cv}^z(\epsilon, \theta)|^2$ term for model 1.

The shift vector is another factor that has topological information about the wave function. The Berry connection explicitly contributes to the shift vector via Eq. (10), which is a gauge-invariant physical quantity. There are intraband and interband contributions to the shift vector, coming from ξ_{nm}^z and $\partial_{k_c} \phi_{nm}^z$, respectively. In our models, in the low-frequency limit, both of these quantities scale as ϵ^{-2+b} . Thus we can write the shift vector as $R_{cv,z}^z = \epsilon^{-2+b} h_{a,b}^{R,zz}(\theta)$. Here, $h_{a,b}^{R,zz}(\theta)$ is an angular part of the shift vector along the z direction in model 1, which depends on both a and b exponents.

Finally, in the low-frequency limit, the simplified form of Eq. (28) [as discussed in Appendix B, Eq. (B17)] can be written as the product of the Jacobian determinant, the transition intensity, and the shift vector. By multiplying these terms we find that the integrand of the shift conductivity shown in Eq. (28) can be written as

$$I^{zzz}(\epsilon, \theta) = \frac{k_0}{\epsilon^{4-b-\frac{1}{a}}} F_{a,b}^{zzz}(\theta) + \frac{1}{\epsilon^{4-b-\frac{2}{a}}} G_{a,b}^{zzz}(\theta). \quad (29)$$

TABLE I. The shift current conductivity for the case of $a = 2$ and $b = 2$ for both model 1 and model 2. For this parameter choice, we can see divergent behavior in both models along the zzz , zxx , and xzx directions. The zzz conductivity has more singular behavior than that of the other directions for both models. Note that in the zzz direction, in model 2, the shift conductivity is independent of k_0 . Here, $\Gamma(x)$ is the Euler gamma function, and $K(x)$ is the complete elliptic integral of the first kind.

Choice of parameters $a = 2$ and $b = 2$		
Shift conductivity	Model 1	Model 2
$\sigma_{\text{shift}}^{zzz}(0; \omega, -\omega)$	$\frac{e^3}{\hbar^2} \frac{2k_0 \sqrt{\frac{2\pi}{\Gamma}} \Gamma(3/4)^2}{\omega^{3/2}}$	$\frac{e^3}{\hbar^2} \frac{\sqrt{\frac{2\pi}{\Gamma}} \Gamma(3/4)^2}{\omega^{3/2}}$
$\sigma_{\text{shift}}^{zxx}(0; \omega, -\omega)$	$\frac{e^3}{\hbar^2} \frac{4\pi k_0 \sqrt{2\Gamma} K(1/2)}{21v_y^2 \omega^{1/2}}$	$\frac{e^3}{\hbar^2} \frac{8\pi k_0^2 \sqrt{2\Gamma} K(1/2)}{21v_y^2 \omega^{1/2}}$
$\sigma_{\text{shift}}^{xzx}(0; \omega, -\omega)$	$\frac{e^3}{\hbar^2} \frac{5\pi k_0 \sqrt{2\Gamma} K(1/2)}{21v_y^2 \omega^{1/2}}$	$\frac{e^3}{\hbar^2} \frac{10\pi k_0^2 \sqrt{2\Gamma} K(1/2)}{21v_y^2 \omega^{1/2}}$

Here, $F_{a,b}^{zzz}(\theta) = h_a(\theta) h^{r,z}(\theta) h^{R,zz}(\theta)$ and $G_{a,b}^{zzz}(\theta) = g_a(\theta) h^{r,z}(\theta) h^{R,zz}(\theta)$. The exact expressions of $F_{a,b}^{zzz}(\theta)$ and $G_{a,b}^{zzz}(\theta)$ can be found in Appendix B, Eqs. (B20) and (B21), respectively.

In the zxx direction, the shift vector and the density of states scale similarly to the way they scale in the zzz direction. However, for the transition intensity, we have $|r_{cv}^x|^2 = \epsilon^{-\frac{2}{a}} h_a^{r,x}(\theta)$. By multiplying all these three quantities, $I^{zxx}(\epsilon, \theta)$ is found as

$$I^{zxx}(\epsilon, \theta) = \frac{k_0}{\epsilon^{2-b+\frac{1}{a}}} F_{a,b}^{zxx}(\theta) + \frac{1}{\epsilon^{2-b}} G_{a,b}^{zxx}(\theta). \quad (30)$$

Here, $F_{a,b}^{zxx}(\theta) = h_a(\theta) h_a^{r,x}(\theta) h^{R,zx}(\theta)$ and $G_{a,b}^{zxx}(\theta) = g_a(\theta) h_a^{r,x}(\theta) h^{R,zx}(\theta)$. The exact expressions of $F_{a,b}^{zxx}$ and $G_{a,b}^{zxx}$ can be found in Appendix B, Eqs. (B14) and (B15), respectively.

For model 2, the evaluation of the shift conductivity would be similar to the case of model 1 in the zzz direction. The shift vector scales as in model 1, $R_{cv,z}^z = \epsilon^{-2+b} \tilde{h}_{a,b}^{R,zz}(\theta)$, and the transition intensity scales as $|r_{cv}^z|^2 = \epsilon^{-2} \tilde{h}^{r,z}(\theta)$. In model 2, the Jacobian of the variable change would be $|\det \tilde{J}| = \tilde{\rho}(\epsilon) \tilde{h}_a$, which is independent of k_0 . By multiplying all these three quantities, we find that the I^{zzz} tensor for model 2 is given by

$$\tilde{I}^{zzz}(\theta, \epsilon) = \frac{1}{\epsilon^{4-b-\frac{1}{a}}} \tilde{F}_{a,b}^{zzz}(\theta). \quad (31)$$

Here, $\tilde{F}_{a,b}^{zzz}(\theta) = \tilde{h}^{r,z}(\theta) \tilde{h}_{a,b}^{R,zz}(\theta) \tilde{h}_a$ [see Appendix B, Eq. (B33), for details]. Note that there is no contribution from k_0 to the shift conductivity in the zzz direction for model 2, and the reason is that the joint-density-of-states equation (27) is independent of k_0 in this model.

In the zxx direction, however, the result depends on k_0^2 as shown in Table I. The k_0 dependence in this direction comes from the transition intensity $|r_{cv}^x|^2 = k_0^2 \epsilon^{-2/a} h_a^{r,x}(\theta) + \epsilon^{-1/a} g_a^{r,x}(\theta)$. Here, $h_a^{r,x}(\theta)$ and $g_a^{r,x}(\theta)$ are the angular parts of the transition intensity. The other two factors, the shift vector and the joint density of states, remain the same as in the zzz direction. Finally, by considering these three terms, we find

that $I^{zx}(\theta, \epsilon)$ can be written as

$$\tilde{I}^{zx}(\theta, \epsilon) = \frac{k_0^2}{\epsilon^{2-b+1/a}} \tilde{F}_{a,b}^{zx}(\theta) + \frac{1}{\epsilon^{2-b}} \tilde{G}_{a,b}^{zx}(\theta). \quad (32)$$

Here, \tilde{F}_{ab}^{zx} and \tilde{G}_{ab}^{zx} are angular-dependent functions similar to \tilde{F}_{ab}^{zz} .

Now we are ready to discuss the overall scaling behavior of the shift conductivity for models 1 and 2. Considering the frequency dependence of all the factors discussed above, one can see that it depends strongly on the choice of the a and b exponents. Let us first investigate the effect of the b coefficient in the shift conductivity. As can be seen from Eq. (29), in order to find the most singular behavior for the shift conductivity, it would be convenient to fix the b exponent as the minimum integer possible. However, for $b = 1$, the Hamiltonian does not break the inversion symmetry, and the shift conductivity would vanish (one can also see that all the angular functions would vanish explicitly for the choice of $b = 1$ as seen in Appendix B). The next relevant choice is $b = 2$, which would break the inversion symmetry of the Hamiltonian, leading to a finite shift conductivity. Hence we use $b = 2$ for the following discussions even though the exponent b is explicitly shown in all the formulas.

For model 1, when a is an even integer, we find that the second term of Eq. (29) vanishes after integrating over θ , and only the first term contributes to the shift conductivity. In this case, we can see that the shift conductivity scales as

$$\sigma_{\text{shift}}^{zzz}(0; \omega, -\omega) \sim k_0 \omega^{-4+b+\frac{1}{a}} \quad (a = \text{even}). \quad (33)$$

If a is an odd integer, then the first term in Eq. (29) vanishes, and only the second term can contribute, leading to

$$\sigma_{\text{shift}}^{zzz}(0; \omega, -\omega) \sim \omega^{-4+b+\frac{2}{a}} \quad (a = \text{odd}). \quad (34)$$

Similar power-law behaviors can be found for the zxx and xzx directions as well. Let us now consider the zxx direction for simplicity, but one can generalize the following argument to the case of the xzx direction. Similar to the zzz direction, when we integrate over θ for an even integer a , only the first term in Eq. (30) survives and the $\tilde{G}_{a,b}^{zx}(\theta)$ would vanish. However, when a is odd, the second term survives and the $\tilde{F}_{a,b}^{zx}(\theta)$ vanishes. Thus we find that the scaling behavior of the shift conductivity in the zxx direction is as follows when a is even:

$$\sigma_{\text{shift}}^{zxx}(0; \omega, -\omega) \sim k_0 \omega^{-2+b-1/a} \quad (a = \text{even}). \quad (35)$$

When a is odd, we have

$$\sigma_{\text{shift}}^{zxx}(0; \omega, -\omega) \sim \omega^{-2+b} \quad (a = \text{odd}). \quad (36)$$

For model 2, the functions $\tilde{F}_{a,b}^{zzz}(\theta)$ and $\tilde{F}_{a,b}^{zxx}(\theta)$ vanish after evaluating the integral over the angular part when a is an odd integer. Hence, for odd integer a , the shift conductivity for the zzz direction vanishes, and the shift conductivity is finite only for even integer a . For the zxx direction, only the $\tilde{G}_{a,b}^{zx}(\theta)$ part contributes for odd integer a , while both terms can contribute in the case of even integer a . Therefore, when a is even, we can write the scaling of the shift conductivity for model 2 as follows.

$$\tilde{\sigma}_{\text{shift}}^{zzz}(0; \omega, -\omega) \sim \omega^{-4+b+\frac{1}{a}} \quad (a = \text{even}), \quad (37)$$

TABLE II. The shift conductivity for the case of $a = 1$ and $b = 2$ for both model 1 and model 2. The conductivities in this case are constant in both models and independent of k_0 .

Choice of parameters $a = 1$ and $b = 2$		
Shift conductivity	Model 1	Model 2
$\sigma_{\text{shift}}^{zzz}(0; \omega, -\omega)$	$\frac{e^3}{\hbar^2} \frac{\pi^2 t_z}{t_x^2}$	0
$\sigma_{\text{shift}}^{zxx}(0; \omega, -\omega)$	$\frac{e^3}{\hbar^2} \frac{\pi^2 t_z}{16v_y^2}$	$\frac{e^3}{\hbar^2} \frac{\pi^2 t_z}{8v_y^2}$
$\sigma_{\text{shift}}^{xzx}(0; \omega, -\omega)$	$\frac{e^3}{\hbar^2} \frac{3\pi^2 t_z}{32v_y^2}$	$\frac{e^3}{\hbar^2} \frac{3\pi^2 t_z}{16v_y^2}$

$$\tilde{\sigma}_{\text{shift}}^{zxx}(0; \omega, -\omega) \sim k_0^2 \omega^{-2+b-\frac{1}{a}} \quad (a = \text{even}). \quad (38)$$

When a is odd, we get

$$\tilde{\sigma}_{\text{shift}}^{zxx}(0; \omega, -\omega) \sim \omega^{-2+b} \quad (a = \text{odd}). \quad (39)$$

As we discussed earlier, we may focus on the choice of $b = 2$ in these models. Now let us consider both the case of $a = 2$, $b = 2$ and the case of $a = 1$, $b = 2$. For models 1 and 2 with $a = 2$, $b = 2$, in the zzz direction, by using Eqs. (33) and (37), we obtain $\sigma_{\text{shift}}^{zzz} \sim k_0/\omega^{3/2}$ and $\tilde{\sigma}_{\text{shift}}^{zzz} \sim 1/\omega^{3/2}$, respectively. In comparison to other systems with singular behavior in the shift conductivity, such as Weyl semimetals, our models show even more singular behavior. In type I and type II Weyl semimetals, $\sigma_{\text{Weyl,I}}^{zzz} \sim \omega^0$ and $\sigma_{\text{Weyl,II}}^{zzz} \sim 1/\omega$ [30], respectively. The exact expression of the shift conductivity of models 1 and 2 in the case of $a = 2$, $b = 2$ can be found in Table I. For the second case, $a = 1$, $b = 2$, we can see that the shift conductivity is constant in both models as shown in Table II.

C. Second-harmonic generation

The SHG in these classes of Hamiltonians is the sum of all four quantities given in Eqs. (12)–(15), which we are going to investigate in detail. For two-band systems, we can simplify the expression of the SHG response as follows.

$$\sigma_{2p,I}^{ijm}(\omega) = \frac{i\pi e^3}{2\hbar^2 \omega^2} \int [dk] M_{2pI,cv}^{ijm}(k) f_{vc} \delta(2\omega - \omega_{cv}), \quad (40)$$

$$\sigma_{2p,II}^{ijm}(\omega) = \frac{i\pi e^3}{2\hbar^2 \omega^2} \int [dk] M_{2pII,cv}^{ijm}(k) f_{vc} \delta(2\omega - \omega_{cv}), \quad (41)$$

$$\sigma_{1p,I}^{ijm}(\omega) = \frac{i\pi e^3}{2\hbar^2 \omega^2} \int [dk] M_{1pI,cv}^{ijm}(k) f_{vc} \delta(\omega - \omega_{cv}), \quad (42)$$

$$\sigma_{1p,II}^{ijm}(\omega) = \frac{i\pi e^3}{2\hbar^2 \omega^2} \int [dk] M_{1pII,cv}^{ijm}(k) f_{vc} \delta(\omega - \omega_{cv}), \quad (43)$$

where

$$M_{2pI,cv}^{ijm} = v_{vc}^i w_{cv}^{jm}, \quad (44)$$

$$M_{2pII,cv}^{ijm} = \frac{-4v_{vc}^i [v_{cv}^j, v_{cc}^m]_+}{\omega_{cv}}, \quad (45)$$

$$M_{1pI,cv}^{ijm} = w_{vc}^{ij} v_{cv}^m + w_{vc}^{im} v_{cv}^j, \quad (46)$$

$$M_{1pII,cv}^{ijm} = \frac{2v_{vc}^i [v_{cc}^j, v_{cv}^m]_+}{\omega_{cv}} - \frac{v_{cc}^i [v_{cv}^j, v_{vc}^m]_+}{\omega_{cv}}, \quad (47)$$

where $[v_{nm}^i, v_{mp}^j]_+ = v_{nm}^i v_{mp}^j + v_{nm}^j v_{mp}^i$ and n, m , and p are the band indices. Note that we used $v_{cc}^i = -v_{vv}^i$, which holds in our models. Note that the imaginary part of M^{ijm} gives rise to the real part of the SHG.

Let us first consider the zzz direction to investigate the effect of each term on the real part of the SHG. In the zzz direction, by using the fact that $v_{cv}^i = v_{vc}^{i*}$, it is easy to see that Eqs. (45) and (47) are completely real and do not contribute to the real part of the SHG. In the zzz direction, $M_{2p,1}^{zzz} = -\frac{1}{2}M_{1p,1}^{zzz}$, which is proportional to $|r_{cv}^z|^2 R_{cv,z}^z$ [see Appendix D, Eq. (D34)]. Thus, remarkably, we can write the SHG response in the zzz direction in terms of the shift conductivity in the zzz direction.

$$\begin{aligned} \text{Re} [\sigma_{\text{SHG}}^{zzz}(2\omega; \omega, \omega)] \\ = \sigma_{\text{shift}}^{zzz}(0; 2\omega, -2\omega) - \frac{1}{2}\sigma_{\text{shift}}^{zzz}(0; \omega, -\omega). \end{aligned} \quad (48)$$

Now we investigate the SHG for the zxx direction. In our choice of Hamiltonians, considering the zxx direction, $M_{1p,1}^{zxx}$ vanishes because there are no crossing terms such as $k_x k_z$ in the Hamiltonian. Thus the finite contributions come from $M_{2p,1}^{zxx}$, $M_{2p,1}^{zxx}$, and $M_{1p,1}^{zxx}$. By some calculations (see Appendix E), we can show that these quantities can be written in terms of the shift conductivity. As a result, the SHG in the zxx direction can be written in terms of the shift conductivity as follows.

$$\begin{aligned} \text{Re} [\sigma_{\text{SHG}}^{zxx}(2\omega; \omega, \omega)] \\ = -3\sigma_{\text{shift}}^{zxx}(0; 2\omega, -2\omega) + 2\sigma_{\text{shift}}^{zxx}(0; 2\omega, -2\omega) \\ + \frac{1}{2}\sigma_{\text{shift}}^{zxx}(0; \omega, -\omega). \end{aligned} \quad (49)$$

Recall that the shift conductivity is related to the shift vector, which is a quantum geometric quantity in momentum space and has topological information about the wave function. Hence, interestingly, the real part of the SHG in both models (models 1 and 2) can also be expressed in terms of such quantum geometric quantities (see Appendix D).

V. SUMMARY AND DISCUSSION

In this paper, we investigated two distinct classes of models of nodal line semimetals with and without inversion symmetry. In both cases, we showed that the nodal line semimetals can produce large nonlinear responses such as SHG and shift current in the low-frequency limit. In the case of a model with inversion symmetry, we apply a dc electric field to break the inversion in the electron distribution, which is necessary to produce a finite nonlinear response. At this point, the NLSM in the presence of an external dc electric field exhibits a large SHG response at finite doping and in the low-frequency limit. It is given by $\sigma_{\text{SHG}}(2\omega; \omega, \omega) \sim k_0/\mu^2$ when $vk_0 > \mu$, which is a more singular response than that of Weyl semimetals. On the other hand, in the regime $vk_0 \ll \mu$, we obtain $\sigma_{\text{SHG}}(2\omega, \omega, \omega) \sim k_0/\mu^2 + 1/\mu$. Note that in the limit $k_0 \rightarrow 0$, the result reduces to the case of Weyl semimetals in an external dc electric field, $\sigma_{\text{SHG}}(2\omega, \omega, \omega) \sim 1/\mu$.

Second, we consider the case without inversion symmetry, and analyze two NLSM models in this class. We compute the shift conductivity and SHG of the two models and find that

the shift conductivity in both models strongly depends on the dispersion relation of the NLSM.

The results are shown in Tables II and I. We also show that the real part of the SHG is related to the shift current as shown in Eqs. (49) and (48). To estimate an order of magnitude of the results in Table I, let us consider the system in the low-temperature-and-low-frequency limit (terahertz regime). Using $\omega \sim 1$ THz, we can see that $\sigma_W = \frac{e^3}{\hbar^2 \omega} \sim 0.01A/V^2$, where σ_W is the conductivity of the type II Weyl semimetal [30]. However, if we choose the exponents $a = 2$ and $b = 2$ in model 1 for the NLSM and consider $t_x \sim t_z$ and $v_y \sim t_x$,

we find that $\sigma_{\text{NLSM}}^{zzz} \sim \sigma_W \sqrt{\left(\frac{t_x k_0^2}{\hbar \omega}\right)}$. In the low-frequency limit, if we choose $\hbar \omega \ll t_x k_0^2 \sim 100\hbar \omega$, we get $\sigma_{\text{NLSM}}^{zzz} \sim 0.1A/V^2$. Hence the response of the NLSM can be an order of magnitude larger than the response of the type II Weyl semimetal. Our results provide an exciting route to generate enhanced nonlinear optical responses in a variety of material platforms exhibiting NLSM behavior. Some examples are HgCr₂Se₄ [35], Cu₃PdN [36], Cu₃ZnN [37], Ca₃P₂ [38], ZrSiS [39], and SrIO₃ [40]. In particular, when the inversion or time-reversal symmetry is broken, the so-called Weyl nodal line semimetals may arise. Recently, noncentrosymmetric 111-type materials, LaNiSi, LaPtSi, and LaPtGe, have been predicted to be Weyl nodal line semimetals [50]. These materials break inversion symmetry and also produce NLSM dispersion, which make them good realizations of the large nonlinear optical responses studied in this paper.

ACKNOWLEDGMENTS

We thank John Sipe for helpful discussions about the consideration of nonlinear responses in the length gauge and velocity gauge. This work was supported by the Natural Sciences and Engineering Research Council of Canada (NSERC) and the Centre for Quantum Materials at the University of Toronto.

APPENDIX A: SECOND-ORDER RESPONSE

Systems with multiband structure exhibit two kinds of polarization due to the interband and intraband interactions, which we will denote as \mathbf{P}_e and \mathbf{P}_i , respectively.

$$\hat{\mathbf{P}} = \hat{\mathbf{P}}_e + \hat{\mathbf{P}}_i, \quad (A1)$$

where

$$\hat{\mathbf{P}}_e = e \int [dk] \sum_{nm} \mathbf{r}_{nm} a_n^\dagger(k) a_m(k), \quad (A2)$$

$$\hat{\mathbf{P}}_i = e \int [dk] \sum_n (a_n^\dagger(k) \partial_{\mathbf{k}} a_n(k) - i \xi_{nn} a_n^\dagger(k) a_n(k)), \quad (A3)$$

and

$$\begin{aligned} \xi_{nm} &= i u_n(k)^* \partial_{\mathbf{k}} u_m(k), \\ \mathbf{r}_{nm} &= \xi_{nm} \quad \text{when } n \neq m. \end{aligned} \quad (A4)$$

Here, \mathbf{r}_{nm} is the off-diagonal element of the position operator, and ξ_{nm} can be considered as the Berry connection of the n th band.

By applying an optical field to the system we can find the linear and nonlinear susceptibility $(\mathbf{P}(\omega_\Sigma)) = \chi_0 + \chi_1 E(\omega_\Sigma) + \chi_2(\omega_\Sigma, \omega_1, \omega_2) E_{\omega_1} E_{\omega_2} + \dots$, where $\omega_\Sigma = \omega_1 + \omega_2$. To find the susceptibility, we need to find the generalized distribution function in the presence of the applied electric field. We define the generalized distribution function as $\rho_{nm} = \langle a_n^\dagger(k) a_m(k) \rangle$ which satisfy the following equation:

$$\frac{\partial \rho_{nm}}{\partial t} + i\omega_{nm}\rho_{nm} = \frac{e}{i\hbar} \sum_{lb} E^b (\rho_{ml} r_{ln}^b - r_{ml}^b \rho_{ln}) - \frac{e}{\hbar} E^b \rho_{mn;b}, \quad (\text{A5})$$

where the the generalized derivative is defined as $\rho_{mn;b} = \partial_{k_b} \rho_{nm} - i(\xi_{nn}^b - \xi_{mm}^b) \rho_{nm}$ and $\omega_{nm} = \omega_n - \omega_m$.

By solving Eq. (A5) perturbatively on the electric field, we can find the nonlinear contributions. Let us consider the following form for the density distribution function:

$$\rho_{nm} = f_n \delta_{nm} + \rho^{(1)} + \rho^{(2)}, \quad (\text{A6})$$

where f_n is the Fermi distribution. $\rho^{(1)}$ shows the first-order contribution, and $\rho^{(2)}$ shows the second-order contribution in the electric field.

By solving Eq. (A5) to the first order in the electric field we can find the following solution:

$$\tilde{\rho}_{nm}^{(1)} = \rho_{\text{FS}}^{(1)} + \rho^{(1)}, \quad (\text{A7})$$

$$\rho_{\text{FS}}^{(1)} = -\delta_{nm} \frac{ie}{\hbar} \sum_{b\beta} \frac{1}{\omega_\beta} \frac{\partial f_n}{\partial k_b} E_\beta^b e^{-i\omega_\beta t}, \quad (\text{A8})$$

$$\rho^{(1)} = \frac{e}{\hbar} \sum_{b\beta} \frac{r_{nm}^b f_{nm}}{\omega_{nm} - \omega_\beta} E_\beta^b e^{-i\omega_\beta t}. \quad (\text{A9})$$

$\rho_{\text{FS}}^{(1)}$ denotes the first-order contribution coming from the Fermi surface of the system at low temperature (because of the derivative of the distribution function). Since the contribution of the Fermi surface is constrained to same-band processes, it will vanish for interband polarization, and we can ignore the contribution of $\rho_{\text{FS}}^{(1)}$ to the interband polarization. For the second-order perturbation we can find the following solution:

$$\rho^{(2)} = \frac{ie}{\hbar(\omega_{nm} - \omega_\Sigma)} \left[\rho_{mn;c}^{(1)} + i \sum_l (\rho_{ml}^{(1)} r_{ln} - r_{ml} \rho_{ln}^{(1)}) \right]. \quad (\text{A10})$$

Finally, by using Eq. (A10) in Eq. (A2) we can find the susceptibilities for the interband contribution as follows:

$$\begin{aligned} \frac{\chi_e^{(2),abc}(\omega_\Sigma; \omega_\beta, \omega_\alpha)}{C} &= i \sum_{nmk} \frac{r_{nm}^a f_{nm}}{\omega_{nm} - \omega_\Sigma} \left(\frac{r_{nm}^b}{\omega_{nm} - \omega_\beta} \right)_{;c} \\ &\quad - \sum_{nlmk} \frac{r_{nm}^a}{\omega_{nm} - \omega_\Sigma} \left(\frac{r_{ml}^b r_{ln}^c f_{lm}}{\omega_{ml} - \omega_\beta} - \frac{r_{ml}^c r_{ln}^b f_{nl}}{\omega_{ln} - \omega_\beta} \right). \quad (\text{A11}) \end{aligned}$$

Here, $C = e^3 / \hbar^2 V$.

To calculate the intraband contribution, it would be convenient to start with the intraband current $\mathbf{J}_i = \mathbf{J} - \mathbf{J}_e$, where \mathbf{J} is the total current and \mathbf{J}_e is the interband current. We can find

the total current as follows:

$$\mathbf{J} = \frac{e}{V} \sum_{nmk} \mathbf{v}_{nm} a_n^\dagger(k) a_m(k), \quad (\text{A12})$$

where V is the volume of the system and $v_{nm}^a = \langle n | \partial_{k_a} H | m \rangle = \omega_{n;a} \delta_{nm} - i\omega_{mn} r_{nm}^a$. For the interband current we have the following expression:

$$\mathbf{J}_e = \frac{-i}{\hbar} [\mathbf{P}_e, H_0] + \frac{i}{\hbar} [\mathbf{P}_e, \mathbf{P}_i + \mathbf{P}_e]. \quad (\text{A13})$$

The contribution of the first term can be written as follows:

$$\frac{-i}{\hbar} [\mathbf{P}_e, H_0] = \frac{e}{V} \sum_{nmk} \omega_{mn} \mathbf{r}_{nm} a_n^\dagger(k) a_m(k). \quad (\text{A14})$$

The contribution of the second term can be written as follows:

$$\begin{aligned} [P_e^a, P_i^b + P_e^b] &= \frac{-ie^2}{V^2} \sum_{nmk} \left(r_{nm;b}^a + i \sum_p (r_{np}^a r_{pm}^b - r_{np}^b r_{pm}^a) \right) \\ &\quad \times a_n^\dagger(k) a_m(k). \quad (\text{A15}) \end{aligned}$$

Finally, by using $\frac{d\mathbf{P}_i}{dt} = \mathbf{J} - \mathbf{J}_e$ we can find the susceptibility for the intraband contribution

$$\begin{aligned} \frac{\chi_i^{abc}(\omega_\Sigma; \omega_\beta, \omega_\alpha)}{C} &= \frac{i}{\omega_\Sigma^2} \sum_{nmk} \frac{\omega_{nm;a} r_{nm}^b r_{nm}^c f_{nm}}{\omega_{nm} - \omega_\beta} \\ &\quad + \frac{1}{i\omega_\Sigma} \sum_{nmk} \frac{r_{nm;a}^c r_{nm}^b f_{nm}}{\omega_{nm} - \omega_\beta}. \quad (\text{A16}) \end{aligned}$$

Shift and injection

By looking at Eqs. (A11) and (A16) we can see that in the dc limit ($\omega_\Sigma \rightarrow 0$) the dominant contribution comes from χ_i ; so we can neglect the χ_e contribution in the dc limit. We can find the shift current and the injection current just by investigating the divergence behavior of Eq. (A16) (the first term is the injection current, and the second term is the shift current); however, it would be more intuitively useful if we look at the intraband currents in the presence of the electric field (which is the dominant contribution).

$$\begin{aligned} J_i^a &= \frac{e}{V} \sum_{nmk} \left[\omega_{n;a} \delta_{nm} - \frac{e}{\hbar} (\mathbf{E} \times \boldsymbol{\Omega}_n)^a \delta_{nm} - \frac{e}{\hbar} \mathbf{E} \cdot \mathbf{r}_{nm;a} \right] \\ &\quad \times a_n^\dagger(k) a_m(k), \quad (\text{A17}) \end{aligned}$$

$$\begin{aligned} J_i^a &= \frac{e}{V} \sum_{nmk} \left[\omega_{n;a} \delta_{nm} - \frac{e}{\hbar} (\mathbf{E} \times \boldsymbol{\Omega}_n)^a \delta_{nm} - \frac{e}{\hbar} \mathbf{E} \cdot \mathbf{r}_{nm;a} \right] \\ &\quad \times (f_n \delta_{nm} + \rho_{\text{FS}}^{(1)} + \rho_{nm}^{(1)} + \rho_{nm}^{(2)} + \rho_{\text{FS}}^{(2)}). \quad (\text{A18}) \end{aligned}$$

Now for the second-order response we have

$$J_{i,I}^a = \sum_{nmk} \omega_{n;a} \delta_{nm} \rho_{nm}^{(2)}, \quad (\text{A19})$$

$$J_{i,II}^a = - \sum_{nmk} \frac{e}{\hbar} \mathbf{E} \cdot \mathbf{r}_{nm;a} \rho_{nm}^{(1)}, \quad (\text{A20})$$

$$J_{i,\text{FS}_1}^a = \sum_{nmk} \omega_{n;a} \delta_{nm} \rho_{\text{FS}}^{(2)}, \quad (\text{A21})$$

$$J_{i,\text{FS}\Pi}^a = - \sum_{nmk} \frac{e}{\hbar} (\mathbf{E} \times \boldsymbol{\Omega}_n)^a \delta_{nm} \rho_{\text{FS}}^{(1)}. \quad (\text{A22})$$

In our model, since we have both inversion and time-reversal symmetry, the Berry curvature will vanish. Since the contribution of the Fermi surface to the shift conductivity in the NLSM is highly related to the Berry curvature [Eq. (A22)], this contribution also will vanish. In a system with finite Berry curvature the contribution of the Fermi surface becomes important and depends on the topology of the Fermi surface [13]. The real part of $J_{i,\text{I}}^a$ and $J_{i,\text{II}}^a$ is responsible for the injection current and shift current, respectively. Two scenarios can lead to BPVEs. In the first scenario the charge carriers relax momentum asymmetrically into the $\pm k$ direction via collisions with electrons, phonons, or impurities, which makes a net current. In the second scenario the light-matter interactions give rise to the BPVEs. In the injection current processes, light pumps carriers into the conduction band asymmetrically at $\pm k$ in the BZ, and this leads to the net current. To explain the injection current in the wave packet approximation, we can consider an electron with velocity v_n^a , and we can define the current as $J^a = \frac{e}{V} \sum_{nk} f_n v_n^a$. By applying an optical field to the system, current-carrying states are injected into the conduction band.

$$\frac{dJ_{\text{inj}}}{dt} = \frac{e}{V} \sum_{nk} \frac{df_n}{dt} v_n^a, \quad (\text{A23})$$

where $\frac{df_n}{dt}$ is given by the Fermi golden rule

$$\frac{df_c}{dt} = \frac{2\pi e^2}{\hbar^2} \sum_v |E(\omega) \cdot r_{cv}|^2 \delta(\omega_{cv} - \omega), \quad (\text{A24})$$

and breaking inversion symmetry $\frac{d}{dt} f_c(k) \neq \frac{d}{dt} f_c(-k)$ allows us to have a net current. c and v are indices related to the conduction and valence bands, respectively. Note that in a system with time-reversal symmetry (such as model 1 [Eq. (24)] and model 2 [Eq. (25)]) the injection current vanishes because it is an odd function under time-reversal symmetry and will change sign under transformation $\omega_\Sigma \rightarrow -\omega_\Sigma$.

In the shift current process, inversion symmetry breaking along with the separation of the center of the charge of the valence and conduction bands gives rise to the net current. The separation of the center of charge makes the dipole velocity oscillation, and the inversion breaking makes the net current be nonzero.

APPENDIX B: SHIFT CURRENT IN MODELS 1 AND 2

For two-band systems, where the induced light is polarized in the b direction, the shift current in Eq. (A16) can be written as follows (see Appendix D):

$$\sigma_{sh}^{\text{abb}}(0; \omega, -\omega) = \frac{\pi e^3}{\hbar^2} \sum_{cv} \int_{\text{BZ}} [dk] I_{cv}^{\text{abb}}(k) f_{cv} \delta(\omega_{cv} - \omega), \quad (\text{B1})$$

where

$$I_{cv}^{\text{abb}}(k) = - \sum_{ijm} \frac{1}{4d^3} \left(d_m d_{i,b} d_{j,ab} - d_m d_{i,b} d_{j,a} \frac{d_{i,b}}{d} \right) \epsilon_{ijm}. \quad (\text{B2})$$

Here, $d_i(k)$ are coefficients of the Pauli matrices in the Hamiltonian equation (D1).

In the following sections we are going to calculate the I^{abb} tensor for both model 1 and model 2 in the zzz and zxx directions.

1. Model 1

Let us only look at the I^{zxx} component for simplicity.

$$I^{zxx} = t_x^3 t_z v_y a (-1 + b) \frac{k_x^2}{4(k_x^2 + k_y^2)} \frac{(\sqrt{k_x^2 + k_y^2} - k_0)^{-2+3a} k_z^b}{[t_x^2 (\sqrt{k_x^2 + k_y^2} - k_0)^{2a} + t_z^2 k_z^{2b} + v_y^2 k_z^2]^{5/2}}. \quad (\text{B3})$$

As we discussed in Sec. IV A the b exponent can break the symmetry if it has been chosen to be an even integer. Also, in Eq. (B3), we can see that the integration of the function over the Brillouin zone is nonvanishing only for the choice of an even b exponent. To proceed, we are going to use an approximation in which $\epsilon \sim \sqrt{(\sqrt{k_x^2 + k_y^2} - k_0)^{2a} + v_y^2 k_z^2}$. As long as $b > 1$ we can neglect the $t_z k_z^b$ term compared with $v_y k_z$ in the low-frequency limit. By this approximation we can use the following variable change:

$$k_z = \frac{1}{v_y} d \cos(\theta),$$

$$\sqrt{k_x^2 + k_y^2} = \pm \left(\frac{1}{t_x} d \sin(\theta) \right)^{1/a} + k_0,$$

$$\theta \in (0, \pi) \text{ for } \pm, \quad (\text{B4})$$

where the determinant of the Jacobi matrix would be

$$\det |J_{\pm}| = \frac{\csc(\theta) \left(\frac{d \sin(\theta)}{t_x} \right)^{1/a} [k_0 \pm \left(\frac{d \sin(\theta)}{t_x} \right)^{1/a}]}{av_y}. \quad (\text{B5})$$

Let us first look at the $+$ sign. Using the variable change equation (B4) in Eq. (B3) in the low-frequency limit, we can find

$$I_+^{zxx} \det |J_+| = t_x^3 t_z v_y a (-1 + b) \csc(\theta) \cos(\phi)^2 \frac{\left(\frac{d \sin(\theta)}{t_x} \right)^{-1+3} \left(\frac{d \cos(\theta)}{v_y} \right)^b [k_0 + \left(\frac{d \sin(\theta)}{t_x} \right)^{1/a}]}{d^5}. \quad (\text{B6})$$

Also we can do the same with the $-$ sign, with which we find the following expression:

$$I_-^{zxx} \det |J_-| = t_x^3 t_z v_y a (-1 + b) \csc(\theta) \cos(\phi)^2 \frac{(-1)^{3a} \left(\frac{d \sin(\theta)}{t_x}\right)^{\frac{-1}{a}+3} \left(\frac{d \cos(\theta)}{v_y}\right)^b \left[k_0 - \left(\frac{d \sin(\theta)}{t_x}\right)^{1/a}\right]}{d^5}, \quad (\text{B7})$$

$$\sigma_{\text{shift}}^{zxx}(0; \omega, -\omega) = \int_0^\infty \int_0^\pi I_+^{zxx} \det |J_+| \delta(2d - \omega) d\theta dd + \int_0^\infty \int_0^\pi I_-^{zxx} \det |J_-| \delta(2d - \omega) d\theta dd. \quad (\text{B8})$$

Let us look at the structure of I_+ ; after integrating over ϕ , we find the following expression:

$$I_+^{zxx} \det |J_+| = \pi t_x^3 t_z v_y a (-1 + b) d^{-2+b-\frac{1}{a}} \left[k_0 + \left(\frac{d \sin(\theta)}{t_x}\right)^{1/a} \right] \left[\csc(\theta) \cos(\phi)^2 \left(\frac{\sin(\theta)}{t_x}\right)^{\frac{-1}{a}+3} \left(\frac{\cos(\theta)}{v_y}\right)^b \right]. \quad (\text{B9})$$

The term proportional to k_0 can produce more singularity in the shift current (in the case in which it is not zero because of the integral on θ , for example, it would be zero when $a = 1$ and $b = 2$). We can write the integral in the following way, which makes it easier to see the behavior of the shift current with respect to the energy d :

$$I_+^{zxx} \det |J_+| = \frac{k_0}{d^{2-b+\frac{1}{a}}} f_{a,b}^{zxx}(\theta) + \frac{1}{d^{2-b}} g_{a,b}^{zxx}(\theta), \quad (\text{B10})$$

where

$$f_{a,b}^{zxx}(\theta) = 3\pi t_x t_z^{1/a} v_y a (1 - b) \times \left[\csc(\theta) \cos(\phi)^2 (\sin(\theta))^{\frac{-1}{a}+3} \left(\frac{\cos(\theta)}{v_y}\right)^b \right] \quad (\text{B11})$$

and

$$g_{a,b}^{zxx}(\theta) = f_{a,b}^{zxx}(\theta) \left(\frac{\sin(\theta)}{t_x}\right)^{1/a}. \quad (\text{B12})$$

Now by considering $I_+^{zxx} \det |J_+| + I_-^{zxx} \det |J_-|$ we can find the $I^{zxx}(\theta, d)$ defined in Eq. (28) as follows:

$$I^{zxx}(\theta, d) = \frac{k_0}{d^{2-b+\frac{1}{a}}} F_{a,b}^{zxx}(\theta) + \frac{1}{d^{2-b}} G_{a,b}^{zxx}(\theta), \quad (\text{B13})$$

where

$$F_{a,b}^{zxx}(\theta) = f_{a,b}^{zxx}(\theta) (1 + (-1)^a), \quad (\text{B14})$$

$$G_{a,b}^{zxx}(\theta) = g_{a,b}^{zxx}(\theta) (1 - (-1)^a). \quad (\text{B15})$$

Note that $F_{a,b}^{zxx}(\theta)$ is finite when the a exponent is an even number and $G_{a,b}^{zxx}(\theta)$ is finite only when the a exponent is an odd number.

We can do the same for the zzz direction.

$$I^{zzz} = t_x t_z v_y \frac{b(1-b) \left(\sqrt{k_x^2 + k_y^2} - k_0\right) k_z^{-2+b}}{4 \left[t_x^2 \left(\sqrt{k_x^2 + k_y^2} - k_0\right)^{2a} + t_z^2 k_z^{2b} + v_y^2 k_z^2 \right]^{3/2}}. \quad (\text{B16})$$

Using the variable change in Eq. (B4), we find that the I^{zzz} tensor can be written as follows:

$$I_+^{zzz} \det |J_+| = \frac{t_x^{-1/a} t_z v_y^{2-b}}{4a} b (-1 + b) \cos(\theta)^{b-2} \times \sin(\theta)^{\frac{1}{a}} d^{-4+b+\frac{1}{a}} \left[k_0 + d^{1/a} \left(\frac{\sin(\theta)}{t_x}\right)^{1/a} \right], \quad (\text{B17})$$

where by separating the angular part of the function we can simplify the above equation as

$$I_+^{zzz} \det |J_+| = \frac{k_0}{d^{4-b-\frac{1}{a}}} f_{a,b}^{zzz}(\theta) + \frac{1}{d^{4-b-\frac{2}{a}}} g_{a,b}^{zzz}(\theta). \quad (\text{B18})$$

By considering $I^{zzz}(\theta, d) = I_+^{zzz} \det |J_+| + I_-^{zzz} \det |J_-|$ we can find

$$I^{zzz}(\theta, d) = \frac{k_0}{d^{4-b-\frac{1}{a}}} F_{a,b}^{zzz}(\theta) + \frac{1}{d^{4-b-\frac{2}{a}}} G_{a,b}^{zzz}(\theta), \quad (\text{B19})$$

where

$$F_{a,b}^{zzz}(\theta) = \frac{t_x^{-1/a} t_z v_y^{2-b}}{4a} b (-1 + b) \cos(\theta)^{b-2} \sin(\theta)^{1/a} \times k_0 (1 + (-1)^a), \quad (\text{B20})$$

$$G_{a,b}^{zzz}(\theta) = \frac{t_x^{-2/a} t_z v_y^{2-b}}{4a} b (-1 + b) \cos(\theta)^{b-2} \times \sin(\theta)^{2/a} (1 - (-1)^a). \quad (\text{B21})$$

2. Model 2

The model 2 Hamiltonian can be written as follows:

$$\tilde{H}(k) = \tilde{t}_x (k_x^2 + k_y^2 - k_0^2)^a \tau_x + v_y k_z \tau_y + t_z k_z^b \tau_z, \quad (\text{B22})$$

where the scalings of τ_x and τ_y are different.

I^{zxx} and I^{zzz} can be written in the following way:

$$I^{zxx} = a^2(1-b)\tilde{t}_x^3 t_z v_y \frac{k_x^2 k_z^b (k_x^2 + k_y^2 - k_0^2)^{-2+3a}}{(\tilde{t}_x^2 (k_x^2 + k_y^2 - k_0^2)^{2a} + v_y^2 k_z^2 + t_z^2 k_z^{2b})^{5/2}}, \quad (\text{B23})$$

$$I^{zzz} = b(1-b)\tilde{t}_x t_z v_y \frac{k_x^2 k_z^{-2+b} (k_x^2 + k_y^2 - k_0^2)^a}{4(\tilde{t}_x^2 (k_x^2 + k_y^2 - k_0^2)^{2a} + v_y^2 k_z^2 + t_z^2 k_z^{2b})^{3/2}}. \quad (\text{B24})$$

In model 2 we use the following transformation:

$$\begin{aligned} k_z &= \frac{1}{v_y} d \cos(\theta), \\ k_x &= \sqrt{\pm \left(\frac{d}{\tilde{t}_x} \sin(\theta) \right)^{\frac{1}{a}} + k_0^2 \cos(\phi)}, \\ k_y &= \sqrt{\pm \left(\frac{d}{\tilde{t}_x} \sin(\theta) \right)^{\frac{1}{a}} + k_0^2 \cos(\phi)}, \\ \theta &\in [0, \pi) \text{ for } \pm, \\ \phi &\in [0, 2\pi). \end{aligned} \quad (\text{B25})$$

The determinant of the Jacobian matrix for this transformation is given by the following expression:

$$\det |J_{\pm}| = \left(\frac{d}{\tilde{t}_x} \right)^{\frac{1}{a}} \frac{\sin(\theta)^{\frac{1}{a}-1}}{2av_y}. \quad (\text{B26})$$

Using the variable change in Eq. (B23) for the transformation, we can find that

$$\begin{aligned} I_+^{zxx} \det |J_+| &= \frac{a(b-1)t_z \tilde{t}_x^{1/a}}{2v_y^b} d^{-2+b-\frac{1}{a}} \cos(\theta)^b \sin(\theta)^{2-1/a} \\ &\times \left[k_0^2 + d^{1/a} \left(\frac{\sin(\theta)}{\tilde{t}_x} \right)^{1/a} \right] \sin(\phi)^2. \end{aligned} \quad (\text{B27})$$

By considering $\tilde{I}^{zxx}(\theta, d) = I_+^{zxx} \det |J_+| + I_-^{zxx} \det |J_-|$ we find

$$\tilde{I}^{zxx}(\theta, d) = \frac{k_0^2}{d^{2-b+\frac{1}{a}}} \tilde{F}_{ab}^{zxx} + \frac{1}{d^{2-b}} \tilde{G}_{ab}^{zxx}, \quad (\text{B28})$$

where

$$\tilde{F}_{ab}^{zxx} = \frac{\pi a(b-1)t_z \tilde{t}_x^{1/a}}{2v_y^b} \cos(\theta)^b \sin(\theta)^{2-1/a} k_0^2 (1 + (-1)^a), \quad (\text{B29})$$

$$\tilde{G}_{ab}^{zxx} = \frac{\pi a(b-1)t_z}{2v_y^b} \cos(\theta)^b \sin(\theta)^2 (1 - (-1)^a). \quad (\text{B30})$$

We can do the same for I^{zzz} , for which we find

$$I_+^{zzz} \det |J_+| = \frac{b(b-1)t_z \tilde{t}_x^{-1/a}}{8av_y^{b-2}} d^{-4+b+\frac{1}{a}} \cos(\theta)^{b-2} \sin(\theta)^{1/a}, \quad (\text{B31})$$

and by considering $\tilde{I}^{zzz}(\theta, d) = I_+^{zzz} \det |J_+| + I_-^{zzz} \det |J_-|$ we can find the final form of $I^{zzz}(\theta, d)$ as follows:

$$\tilde{I}^{zzz}(\theta, d) = \frac{1}{d^{4-b-\frac{1}{a}}} \tilde{F}_{ab}^{zzz}, \quad (\text{B32})$$

TABLE III. The coefficients of Eq. (20) for different directions ($a, b, c \in \{x, z\}$). Note that the other four directions (zxx, zxz, xzz, xxx) that are not included in the table vanish.

Coefficients of the 1pII and 2pII resonances		
abc	C_{1pII}^{abc}	C_{2pII}^{abc}
zzz	$-\pi^2$	$\frac{\pi^2}{16}$
zxx	$\frac{\pi^2}{2}$	$-\frac{5\pi^2}{32}$
xzx	$-\frac{\pi^2}{2}$	$\frac{3\pi^2}{32}$
xxz	$\frac{-\pi^2}{2}$	$\frac{3\pi^2}{32}$

$$\tilde{F}_{a,b}^{zzz}(\theta) = \frac{b(b-1)t_z \tilde{t}_x^{-1/a}}{8av_y^{b-2}} \cos(\theta)^{b-2} \sin(\theta)^{1/a} (1 + (-1)^a). \quad (\text{B33})$$

APPENDIX C: SECOND-HARMONIC GENERATION IN A NODAL LINE SEMIMETAL

Consider a general Hamiltonian written in the form of Eq. (D1). The inversion-symmetric Hamiltonian in Eq. (16) is a particular choice for $d_x = v(\sqrt{k_x^2 + k_y^2} - k_0)$, $d_y = 0$, and $d_z = vk_z$.

Note that in an inversion-symmetric system we need an external electric field to break the inversion symmetry in order to find the second-order response in the system. Let us assume that the external electric field is in the z direction. This external electric field changes the electron distribution function in the conduction and valence bands, which we can write as follows up to the first order in the external electric field:

$$f_n = f_n^{(0)} + \frac{e\tau}{\hbar} E_z \partial_{k_z} \epsilon \frac{\partial f_n^{(0)}(\epsilon)}{\partial \epsilon(k)}. \quad (\text{C1})$$

Here, $f_n^{(0)}(\epsilon)$ is the equilibrium distribution function, n is the band index, and ϵ is the conduction band's energy.

There are four contributions to the SHG in Eqs. (40)–(43) for two-band systems which we are going to investigate for Hamiltonian equation (16).

$$\sigma_{2p,I}^{ijm}(\omega) = \frac{e^3}{2\hbar^2\omega^2} \int [dk] M_{2pI,cv}^{ijm}(k) f_{vc} R_Y(2\omega - \omega_{cv}), \quad (\text{C2})$$

$$\sigma_{2p,II}^{ijm}(\omega) = \frac{e^3}{2\hbar^2\omega^2} \int [dk] M_{2pII,cv}^{ijm}(k) f_{vc} R_Y(2\omega - \omega_{cv}), \quad (\text{C3})$$

$$\sigma_{1p,I}^{ijm}(\omega) = \frac{e^3}{2\hbar^2\omega^2} \int [dk] M_{1pI,cv}^{ijm}(k) f_{vc} R_Y(2\omega - \omega_{cv}), \quad (\text{C4})$$

$$\sigma_{1p,II}^{ijm}(\omega) = \frac{e^3}{2\hbar^2\omega^2} \int [dk] M_{1pII,cv}^{ijm}(k) f_{vc} R_Y(2\omega - \omega_{cv}), \quad (\text{C5})$$

where

$$M_{2pI,cv}^{ijm} = v_{vc}^i w_{cv}^{jm}, \quad (\text{C6})$$

$$M_{2pII,cv}^{ijm} = \frac{-4v_{vc}^i [v_{cv}^j, v_{cc}^m]_+}{\omega_{cv}}, \quad (\text{C7})$$

$$M_{1pI,cv}^{ijm} = w_{vc}^{ij} v_{cv}^m + w_{vc}^{im} v_{cv}^j, \quad (\text{C8})$$

$$M_{1pII}^{ijm} = \frac{2v_{vc}^i}{\omega_{cv}} [v_{cc}^j, v_{cv}^m]_+ - \frac{v_{cc}^i}{\omega_{cv}} [v_{cv}^j, v_{vc}^m]_+ \quad (C9)$$

and $w^{ab} = (1/\hbar)\partial_{k_a}\partial_{k_b}H$, $[v_{np}^b v_{pm}^c]_+ = v_{np}^b v_{pm}^c + v_{np}^c v_{pm}^b$, and $R_\gamma(x) = 1/(x - i\gamma)$, where γ is related to the decay rate.

Let us consider $|1\rangle$ as the conduction band and $|0\rangle$ as the valence band. Using the following identity for Pauli matrices, τ_i , we can find the general form of M_I and M_{II} for the 2×2 Hamiltonians ($H = \sum_{\alpha=1}^3 d_\alpha \tau_\alpha$):

$$\langle 0|\tau_\alpha|1\rangle\langle 1|\tau_\beta|0\rangle = \left(\delta_{ij} - \frac{d_\alpha d_\beta}{d^2}\right) - i\epsilon_{\alpha\beta\gamma} \frac{d_\gamma}{d}. \quad (C10)$$

Thus we have

$$\begin{aligned} v_{vc}^i v_{cv}^j &= \frac{\partial d_\alpha}{\partial k_i} \frac{\partial d_\beta}{\partial k_j} \langle 0|\tau_\alpha|1\rangle\langle 1|\tau_\beta|0\rangle \\ &= \frac{\partial d_\alpha}{\partial k_i} \frac{\partial d_\beta}{\partial k_j} \left[\left(\delta_{\alpha\beta} - \frac{d_\alpha d_\beta}{d^2}\right) - i\frac{d_\gamma}{d} \epsilon_{\alpha\beta\gamma} \right], \end{aligned} \quad (C11)$$

$$\begin{aligned} v_{vc}^i w_{cv}^{jm} &= \frac{\partial d_\alpha}{\partial k_i} \frac{\partial^2 d_\beta}{\partial k_j \partial k_m} \langle 0|\tau_\alpha|1\rangle\langle 1|\tau_\beta|0\rangle \\ &= \frac{\partial d_\alpha}{\partial k_i} \frac{\partial^2 d_\beta}{\partial k_j \partial k_m} \left[\left(\delta_{\alpha\beta} - \frac{d_\alpha d_\beta}{d^2}\right) - i\frac{d_\gamma}{d} \epsilon_{\alpha\beta\gamma} \right]. \end{aligned} \quad (C12)$$

Using Eqs. (C11) and (C12) in Eqs. (C6)–(C9) and separating the imaginary and real parts of each function, we find

$$\text{Re} [M_{2pI}^{ijm}] = \frac{\partial d_\alpha}{\partial k_i} \frac{\partial^2 d_\beta}{\partial k_j \partial k_m} \left(\delta_{\alpha\beta} - \frac{d_\alpha d_\beta}{d^2}\right), \quad (C13)$$

$$\text{Im} [M_{2pI}^{ijm}] = -\frac{\partial d_\alpha}{\partial k_i} \frac{\partial^2 d_\beta}{\partial k_j \partial k_m} \frac{d_\gamma}{d} \epsilon_{\alpha\beta\gamma}, \quad (C14)$$

$$\text{Re} [M_{2pII}^{ijm}] = \frac{-2}{d} \frac{\partial d_\alpha}{\partial k_i} \left(\frac{\partial d_\beta}{\partial k_j} \frac{\partial d}{\partial k_m} + \frac{\partial d_\beta}{\partial k_m} \frac{\partial d}{\partial k_j} \right) \left(\delta_{\alpha\beta} - \frac{d_\alpha d_\beta}{d^2}\right), \quad (C15)$$

$$\text{Im} [M_{2pII}^{ijm}] = \frac{2}{d} \frac{\partial d_\alpha}{\partial k_i} \left(\frac{\partial d_\beta}{\partial k_j} \frac{\partial d}{\partial k_m} + \frac{\partial d_\beta}{\partial k_m} \frac{\partial d}{\partial k_j} \right) \frac{d_\gamma}{d} \epsilon_{\alpha\beta\gamma}, \quad (C16)$$

$$\text{Re} [M_{1pI}^{ijm}] = \left(\frac{\partial d_\beta}{\partial k_m} \frac{\partial^2 d_\alpha}{\partial k_i \partial k_j} + (j \leftrightarrow m) \right) \left(\delta_{\alpha\beta} - \frac{d_\alpha d_\beta}{d^2}\right), \quad (C17)$$

$$\text{Im} [M_{1pI}^{ijm}] = -\left(\frac{\partial d_\beta}{\partial k_m} \frac{\partial^2 d_\alpha}{\partial k_i \partial k_j} + (j \leftrightarrow m) \right) \frac{d_\gamma}{d} \epsilon_{\alpha\beta\gamma}, \quad (C18)$$

$$\begin{aligned} \text{Re} [M_{1pII}^{ijm}] &= \frac{1}{d} \left(\frac{\partial d_\alpha}{\partial k_i} \frac{\partial d_\beta}{\partial k_m} \frac{\partial d}{\partial k_j} + (j \leftrightarrow m) \right) \left(\delta_{\alpha\beta} - \frac{d_\alpha d_\beta}{d^2}\right) \\ &\quad - \frac{1}{d} \frac{\partial d}{\partial k_i} \frac{\partial d_\beta}{\partial k_m} \frac{\partial d_\alpha}{\partial k_j} \left(\delta_{\alpha\beta} - \frac{d_\alpha d_\beta}{d^2}\right), \end{aligned} \quad (C19)$$

$$\text{Im} [M_{1pII}^{ijm}] = \frac{-1}{d^2} \left(\frac{\partial d_\alpha}{\partial k_i} \frac{\partial d_\beta}{\partial k_m} \frac{\partial d}{\partial k_j} + (j \leftrightarrow m) \right) d_\gamma \epsilon_{\alpha\beta\gamma}. \quad (C20)$$

Note that there is a sum on repeated indices (α , β , and γ). It is easy to see that because $d_\gamma = 0$, all the imaginary parts vanish in the inversion-symmetric NLSM Hamiltonian equation (16). At the low-frequency limit the contributions of M_{2pI}^{ijm} and M_{1pI}^{ijm} to the SHG vanish and only M_{2pII} and M_{1pII}

have finite contributions. Let us consider the zzz direction. In this direction, M_{1pI}^{zzz} and M_{2pI} vanish explicitly because the Hamiltonian is linear in k_z . For M_{2pII} and M_{1pII} we have the following expressions:

$$\text{Re} [M_{2pII}^{zzz}] = \frac{-4(\sqrt{k_x^2 + k_y^2} - k_0)^2 k_z v^2}{((\sqrt{k_x^2 + k_y^2} - k_0)^2 + k_z^2)^2}, \quad (C21)$$

Also it can be seen that $\text{Re}[M_{1pII}^{zzz}] = -\frac{1}{4}\text{Re}[M_{2pII}^{zzz}]$. Now let us use the following variable change:

$$\begin{aligned} k_x &= \left(\frac{d \sin(\theta)}{v} + k_0 \right) \sin(\phi), \\ k_y &= \left(\frac{d \sin(\theta)}{v} + k_0 \right) \cos(\phi), \\ k_z &= \frac{d \cos(\theta)}{v}, \end{aligned} \quad (C22)$$

where the determinant of the above transformation is given by

$$\det |J| = \frac{d(vk_0 + d \sin(\theta))}{v^2}, \quad (C23)$$

where $d = v\sqrt{(\sqrt{k_x^2 + k_y^2} - k_0)^2 + k_z^2}$. Using the above variable change, we can simplify Eq. (C21) as follows:

$$\text{Re} [M_{2pII}^{zzz}] = \frac{-4v^3 \cos(\theta) \sin(\theta)^2}{d}. \quad (C24)$$

Inserting Eq. (C24) into Eq. (C3), we can find

$$\begin{aligned} \sigma_{2p,II}^{zzz} &= \frac{-e^4 E_z v \tau}{2h^3 \omega^2} \int_0^\infty dd \int_0^{2\pi} d\theta \int_0^{2\pi} d\phi (k_0 v + d \sin(\theta)) \\ &\quad \times \sin(2\theta)^2 R_\gamma(2\omega - 2d) \delta(d - \mu). \end{aligned} \quad (C25)$$

The only term that has a finite contribution is the term proportional to k_0 , and the rest vanish due to the angular integral. Thus we find

$$\sigma_{2p,II}^{zzz} = -\frac{e^4 E_z k_0 \pi^2 v^2 \tau}{h^3 \omega^2} R_\gamma(2\omega - 2\mu). \quad (C26)$$

Also by using $\text{Re}[M_{1pII}^{zzz}] = -\frac{1}{4}\text{Re}[M_{2pII}^{zzz}]$, for σ_{1pII}^{zzz} we can find the following expression:

$$\sigma_{1p,II}^{zzz} = \frac{e^4 E_z k_0 \pi^2 v^2 \tau}{4h^3 \omega^2} R_\gamma(\omega - 2\mu). \quad (C27)$$

In the zxx direction, M_{1pI}^{zxx} vanishes explicitly, but M_{2pI} is not explicitly zero. However, the angular integral makes this term vanish. Thus the only contributors come from M_{1pII}^{zxx} and M_{2pII}^{zxx} . By changing the variables [Eq. (C22)] we can simply write the two contributions as follows:

$$\begin{aligned} \sigma_{2p,II}^{zxx} &= \frac{e^4 E_z v \tau}{2h^3 \omega^2} \int_0^\infty dd \int_0^{2\pi} d\theta \int_0^{2\pi} d\phi (k_0 v + d \sin(\theta)) \\ &\quad \times \sin(2\theta)^2 \sin(\phi)^2 R_\gamma(2\omega - 2d) \delta(d - \mu), \end{aligned} \quad (C28)$$

$$\begin{aligned} \sigma_{1p,II}^{zxx} &= \frac{e^4 E_z v \tau}{2h^3 \omega^2} \int_0^\infty dd \int_0^{2\pi} d\theta \int_0^{2\pi} d\phi (k_0 v + d \sin(\theta)) \\ &\quad \times \cos(\theta)^2 (-3 + \cos(2\theta)) \sin(\phi)^2 \\ &\quad \times R_\gamma(\omega - 2d) \delta(d - \mu). \end{aligned} \quad (C29)$$

By evaluating the integrals we find

$$\sigma_{2p,\text{II}}^{xx} = \frac{e^4 E_z \tau \pi^2 k_0 v^2}{2h^3 \omega^2} R_Y (2\omega - 2\mu), \quad (\text{C30})$$

$$\sigma_{1p,\text{II}}^{xx} = \frac{-5e^4 E_z \tau \pi^2 k_0 v^2}{8h^3 \omega^2} R_Y (\omega - 2\mu). \quad (\text{C31})$$

The same approach can be used to find the SHG in the xxz and xzx directions, for which we find the following expressions:

$$\sigma_{2p,\text{II}}^{xxz} = \sigma_{2p,\text{II}}^{xzx} = -\frac{e^4 E_z \tau \pi^2 k_0 v^2}{2h^3 \omega^2} R_Y (2\omega - 2\mu), \quad (\text{C32})$$

$$\sigma_{1p,\text{II}}^{xxz} = \sigma_{1p,\text{II}}^{xzx} = \frac{3e^4 E_z \tau \pi^2 k_0 v^2}{8h^3 \omega^2} R_Y (\omega - 2\mu). \quad (\text{C33})$$

APPENDIX D: DEFINITIONS AND THE SHG AND SHIFT CURRENT RELATION

1. Definitions

A Hamiltonian is defined as

$$H(k) = \sum_{\alpha=1}^3 d_{\alpha}(k) \sigma_{\alpha}, \quad (\text{D1})$$

where $\sigma_1 = \sigma_x$, $\sigma_2 = \sigma_y$, and $\sigma_3 = \sigma_z$ are Pauli matrices.

Shift conductivity is defined as

$$\sigma_{\text{shift}}^{ijm}(0; \omega, -\omega) = \frac{2\pi e^3}{\hbar^2} \int [dk] I_{10}^{ijm} f_{01} \delta(\omega - \omega_{10}), \quad (\text{D2})$$

where 1 and 0 denote the conduction band and the valence band, respectively, and for tensor I_{10}^{ijm} we have (we ignore the index 10 for the I_{10}^{ijm} tensor for simplicity)

$$I^{ijm} = \frac{-1}{2} \text{Im} [r_{10}^j r_{01i}^m + r_{10}^m r_{01i}^j]. \quad (\text{D3})$$

Here, $r_{01i}^m = \partial_{k_i} r_{01}^m - i(\xi_{00}^i - \xi_{11}^i) r_{01}^m$ is the generalized derivative. To see the effect of Berry curvature, we can expand the I tensor

$$I^{ijm} = \frac{1}{2} |r_{10}^j| |r_{01}^m| \left[(\partial_{k_i} (\phi^j + \phi^m) - 2(\xi_{00}^i - \xi_{11}^i)) \cos(\phi^j - \phi^m) + \frac{1}{2} |r_{10}^j|^2 \partial_{k_i} \left(\frac{|r_{01}^m|}{|r_{10}^j|} \right) \sin(\phi^j - \phi^m) \right], \quad (\text{D4})$$

where $\phi^j = \arg(r_{10}^j)$. We can see when j and m are in the same direction, then the sine term vanishes, and the first term becomes the shift vector definition $R_{10,j}^i = \partial_{k_i} \phi^j - (\xi_{00}^i - \xi_{11}^i)$.

We can define I^{ijm} in terms of the Hamiltonian terms as follows:

$$I_{10}^{ijm} = \frac{-1}{8d^3} \sum_{\alpha\beta\gamma} \left[d_{\gamma} d_{\alpha,j} d_{\beta,im} - d_{\alpha,j} d_{\beta,i} d_{\gamma} \frac{d,m}{d} + (j \leftrightarrow m) \right] \times \epsilon_{\alpha\beta\gamma}, \quad (\text{D5})$$

or equivalently we can write the I^{ijm} tensor as

$$I^{ijm} = \frac{1}{\omega_{10}^2} \text{Im} \left(\frac{-v_{10}^i [v_{01}^j v_{11}^m]_+}{\omega_{10}} + \frac{1}{2} (v_{01}^m w_{10}^{ij} + v_{01}^j w_{10}^{im}) \right). \quad (\text{D6})$$

Proof 1. In Proof 1 we show that Eq. (D3) is equal to Eq. (D6). To find r_{nm}^i , we can start with taking the derivative of the Hamiltonian

$$\partial_{k_i} \langle n | H | m \rangle = \epsilon_m \langle \partial_{k_i} n | m \rangle + \langle n | \partial_{k_i} H | m \rangle + \epsilon_n \langle n | \partial_{k_i} m \rangle = 0 \quad (\text{for } n \neq m). \quad (\text{D7})$$

By using the fact that $\langle \partial_{k_i} n | m \rangle = -\langle n | \partial_{k_i} m \rangle$ and using the definition that $r_{nm} = i \langle n | \partial_{k_i} m \rangle$ and $v_{nm}^i = \frac{1}{\hbar} \langle n | \partial_{k_i} H | m \rangle$ we can find

$$i r_{nm} = \frac{v_{nm}}{\omega - \omega_m}. \quad (\text{D8})$$

Now we can take the derivative of Eq. (D8), in which we have

$$i r_{nm;i}^j = \frac{v_{nm;i}^j}{\omega_{nm}} - \frac{v_{nm}^j}{\omega_{nm}^2} \partial_{k_i} \omega_{nm}. \quad (\text{D9})$$

We can define the derivative of the element of the velocity operator as follows:

$$\partial_{k_i} v_{nm} = \partial_{k_i} (\langle n | \hat{v} | m \rangle) = \langle \partial_{k_i} n | \hat{v} | m \rangle + \langle n | \partial_{k_i} \hat{v} | m \rangle + \langle n | \hat{v} | \partial_{k_i} m \rangle. \quad (\text{D10})$$

By inserting the identity operator we can find

$$\begin{aligned} \partial_{k_i} v_{nm}^j &= w_{nm}^{ij} + \langle \partial_{k_i} n | n \rangle v_{nm}^j + \sum_{p \neq n} \langle \partial_{k_i} n | p \rangle v_{pm}^j \\ &+ \sum_{p \neq m} v_{np}^j \langle p | \partial_{k_i} m \rangle + v_{nm}^j \langle m | \partial_{k_i} m \rangle. \end{aligned} \quad (\text{D11})$$

Thus we have

$$\partial_{k_i} v_{nm}^j = w_{nm}^{ij} + i(\xi_{nn}^i - \xi_{mm}^i) v_{nm}^j - i \sum_{p \neq m} v_{np}^j \xi_{pm}^i + i \sum_{p \neq n} \xi_{np}^i v_{pm}^j. \quad (\text{D12})$$

Using the definition of the generalized derivative, we have

$$\begin{aligned} v_{nm;i}^j &= \partial_{k_i} v_{nm}^j - i(\xi_{nn}^i - \xi_{mm}^i) v_{nm}^j \\ v_{nm}^j &= w_{nm}^{ij} - i \sum_{p \neq m} v_{np}^j \xi_{pm}^i + i \sum_{p \neq n} \xi_{np}^i v_{pm}^j; \end{aligned} \quad (\text{D13})$$

also, using the fact that $i r_{nm}^i = \frac{v_{nm}^i}{\omega_{nm}}$ for $n \neq m$ for a two-band system, we have

$$v_{01;i}^j = w_{01}^{ij} + \frac{v_{01}^i (v_{11}^j - v_{00}^j)}{\omega_{01}}. \quad (\text{D14})$$

Inserting Eq. (D14) into Eq. (D9) for a two-band system, we have

$$i \omega_{01} r_{01;i}^j = w_{01}^{ij} + \frac{v_{01}^i (v_{11}^j - v_{00}^j)}{\omega_{01}} + \frac{v_{01}^i (v_{11}^j - v_{00}^j)}{\omega_{01}}. \quad (\text{D15})$$

Finally, by inserting Eq. (D15) into Eq. (D3) we can find Eq. (D6).

Proof 2. In Proof 2 we show that (D6) is equal to (D5). Let us consider only the following part:

$$\frac{1}{\omega_{10}^2} \text{Im} \left[\frac{-v_{10}^i v_{01}^j v_{11}^m}{\omega_{10}} + \frac{1}{2} v_{01}^j w_{10}^{im} \right]. \quad (\text{D16})$$

The other terms will be generated by $(j \leftrightarrow m)$. We can simplify the above expression using the definitions $v_{nm}^i =$

$\frac{1}{\hbar}\langle n|\partial_{k_j}H|m\rangle$, $v_{nm}^j = \frac{1}{\hbar}\langle n|\partial_{k_i}\partial_{k_j}H|m\rangle$, and $\omega_{10} = 2d/\hbar$, in which we find

$$\frac{1}{4d^2} \text{Im} \left[\frac{-1}{2d} \partial_{k_i} d_\alpha \partial_{k_j} d_\beta \langle 1|\sigma_\alpha|0\rangle \langle 0|\sigma_\beta|1\rangle \partial_{k_m} d_\rho \langle 1|\sigma_\rho|1\rangle + \frac{1}{2} \partial_{k_m} d_\alpha \partial_{k_i} \partial_{k_j} d_\beta \langle 0|\sigma_\alpha|1\rangle \langle 1|\sigma_\beta|0\rangle \right]. \quad (\text{D17})$$

Using the following identities, we can simplify the above equation:

$$\langle 1|\sigma_\alpha|0\rangle \langle 0|\sigma_\beta|1\rangle = \left(\delta_{\alpha\beta} - \frac{d_\alpha d_\beta}{d^2} \right) + i\epsilon_{\alpha\beta\gamma} \frac{d_\gamma}{d}, \quad (\text{D18})$$

$$\langle 1|\sigma_\alpha|1\rangle = \frac{d_\alpha}{d}. \quad (\text{D19})$$

Here, $\epsilon_{\alpha\beta\gamma}$ is the Levi-Civita symbol. Now by considering the imaginary part of Eq. (D17) we find

$$\frac{1}{4d^2} \left[-\partial_{k_i} d_\alpha \partial_{k_j} d_\beta \frac{d_l d_\gamma}{2d^2} \partial_{k_m} d_l - \partial_{k_m} \partial_{k_i} \partial_{k_j} d_\beta \partial d_\alpha \frac{d_\gamma}{2d} \right] \epsilon_{\alpha\beta\gamma}. \quad (\text{D20})$$

By changing the α and β indices in the first term and using the identity $d_l \partial_{k_m} d_l = d \partial_{k_m} d$ we can find

$$\frac{-1}{8d^3} \sum_{\alpha\beta\gamma} \left[d_\gamma d_{\alpha,j} d_{\beta,im} - d_{\alpha,j} d_{\beta,i} d_\gamma \frac{d, m}{d} \right] \epsilon_{\alpha\beta\gamma}, \quad (\text{D21})$$

which is the first term in Eq. (D21).

2. SHG and shift current relation

Let us look at the general case of $\sigma_{\text{SHG}}^{ijj}$. Because of the symmetry of the Hamiltonian between x and y in our model, we consider i and j to be z or x only. For the SHG response in the ijj direction we have

$$M_{2pl}^{ijj} = v_{01}^j w_{10}^{jj}, \quad (\text{D22})$$

$$M_{2pII}^{ijj} = \frac{-8v_{01}^i v_{10}^j v_{11}^j}{\omega_{10}}, \quad (\text{D23})$$

$$M_{1pl}^{ijj} = 2w_{01}^{ij} v_{10}^j, \quad (\text{D24})$$

$$M_{1pII}^{ijj} = 4 \frac{v_{01}^i v_{10}^j v_{11}^j}{\omega_{10}} - \frac{2v_{11}^i v_{10}^j v_{01}^j}{\omega_{10}}. \quad (\text{D25})$$

Here, 0 and 1 denote the valence band and the conduction band, respectively. Now we consider two cases: first, the case that $i \neq j$ and, second, the case that $i = j$. For the first case, in our system, w_{01}^{ij} vanishes because there is no crossing term such as $k_x k_z$ in the Hamiltonian. Also the imaginary part of the second term in Eq. (D24) vanishes because it is fully real.

Now let us look at the shift conductivity in the ijj and jij directions.

$$\omega_{10}^2 I^{ijj} = \text{Im} \left[\frac{-2v_{10}^i v_{01}^j v_{11}^j}{\omega_{10}} + v_{01}^j w_{10}^{ij} \right], \quad (\text{D26})$$

$$\omega_{10}^2 I^{jij} = \text{Im} \left[\frac{-v_{10}^j v_{01}^i v_{11}^j}{\omega_{10}} - \frac{v_{10}^j v_{01}^j v_{11}^i}{\omega_{10}} + \frac{1}{2} v_{01}^j w_{10}^{ij} + \frac{1}{2} v_{01}^i w_{10}^{jj} \right]. \quad (\text{D27})$$

Here, we can see that the second term in Eq. (D27) is completely real, and the third term vanishes because, in our system, we do not have crossing terms ($i \neq j$). Thus we can see that we can simplify the above equations as follows:

$$\begin{aligned} \omega_{10}^2 I^{ijj} &= \frac{-1}{4} \text{Im} [M_{2pII}^{ijj}] = \frac{1}{2} \text{Im} [M_{1pII}^{ijj}] \\ &= \text{Im} \left[\frac{-v_{10}^j v_{01}^i v_{11}^j}{\omega_{10}} \right], \end{aligned} \quad (\text{D28})$$

$$\text{Im} [M_{2pl}^{ijj}] = \text{Im} [v_{01}^i w_{10}^{jj}] = 2\omega_{10}^2 I^{jij} + \omega_{10}^2 I^{ijj}. \quad (\text{D29})$$

Now we are able to find the SHG as follows:

$$\sigma_{\text{SHG}}^{ijj}(2\omega; \omega, \omega) = \frac{i\pi e^3}{2\hbar^2 \omega^2} \int [dk] \left((M_{2pII}^{ijj} + M_{2pl}^{ijj}) \delta(2\omega - \omega_{10}) + M_{1pII}^{ijj} \delta(\omega - \omega_{10}) \right) f_{01}. \quad (\text{D30})$$

Using Eqs. (D28) and (D29), we can find that

$$\text{Re} [\sigma_{\text{SHG}}^{ijj}(2\omega; \omega, \omega)] = \frac{\pi e^3}{2\hbar^2 \omega^2} \int [dk] \left(\omega_{10}^2 (-3I^{ijj} + 2I^{jij}) \delta(2\omega - \omega_{10}) + 2\omega_{10}^2 I^{ijj} \right) f_{01}; \quad (\text{D31})$$

we can simplify the ω^2 term in the denominator using the delta function (note that it gives a factor of 4 for the two-photon resonance processes)

$$\text{Re} [\sigma_{\text{SHG}}^{ijj}(2\omega; \omega, \omega)] = \frac{\pi e^3}{\hbar^2} \int [dk] \left(2(-3I^{ijj} + 2I^{jij}) \delta(2\omega - \omega_{10}) + I^{ijj} \right) f_{01}, \quad (\text{D32})$$

and thus by the definition of the shift conductivity we have

$$\text{Re} [\sigma_{\text{SHG}}^{ijj}(2\omega; \omega, \omega)] = -3\sigma_{\text{shift}}^{ijj}(0; 2\omega, -2\omega) + 2\sigma_{\text{shift}}^{jij}(0; 2\omega, -2\omega) + \frac{1}{2}\sigma_{\text{shift}}^{ijj}(0; \omega, -\omega). \quad (\text{D33})$$

For the case that $i = j$, Eqs. (D22) and (D25) vanish because both are real. For the remaining terms we have

$$\text{Im} [M_{2pl}^{iii}] = -\frac{1}{2} \text{Im} [M_{1pl}^{iii}] = \omega_{10}^2 I^{iii}. \quad (\text{D34})$$

Thus we have

$$\text{Re} [\sigma_{\text{SHG}}^{iii}(2\omega; \omega, \omega)] = \frac{\pi e^3}{2\hbar^2 \omega^2} \int [dk] \left(\omega_{10}^2 I^{iii} \delta(2\omega - \omega_{10}) - 2\omega_{10}^2 I^{iii} \delta(\omega - \omega_{10}) \right) f_{01}, \quad (\text{D35})$$

and we can simplify the ω^2 term in the denominator using the delta function, in which we find

$$\text{Re} [\sigma_{\text{SHG}}^{iii}(2\omega; \omega, \omega)] = \sigma_{\text{shift}}^{iii}(0; 2\omega, -2\omega) - \frac{1}{2}\sigma_{\text{shift}}^{iii}(0; \omega, -\omega). \quad (\text{D36})$$

APPENDIX E: SHG IN THE LENGTH GAUGE

It is well known that the calculation of nonlinear responses in the velocity gauge might give rise to unphysical divergences at zero frequencies using the finite-band approximation. However, there is no evidence of finding these unphysical divergences in the length gauge calculation. In this Appendix, for the consistency of this paper we are going to compute the singular behavior of the SHG in the length gauge and compare it with the velocity gauge.

The SHG response in the length gauge can be written as follows [51,52]:

$$\sigma_{\text{SHG}}^{abc,\text{inter}}(2\omega; \omega, \omega) = \frac{2\omega e^3}{\hbar^2} \int [dk] \sum_{cvn} \frac{r_{vc}^a [r_{cn}^b r_{nv}^c]_+}{\omega_{nv} - \omega_{cn}} \left(\frac{2f_{vc}}{\omega_{cv} - 2\omega} + \frac{f_{nc}}{\omega_{nc} - \omega} + \frac{f_{vn}}{\omega_{vn} - \omega} \right), \quad (\text{E1})$$

$$\begin{aligned} \sigma_{\text{SHG}}^{abc,\text{intra}}(2\omega; \omega, \omega) &= \frac{2\omega e^3}{\hbar^2} \int [dk] \sum_{cv} f_{vc} \left[\frac{2}{\omega_{cv}(\omega_{cv} - 2\omega)} r_{vc}^a r_{cv;c}^b + \frac{1}{\omega_{cv}(\omega_{cv} - \omega)} r_{vc;c}^a r_{cv}^b \right. \\ &\quad \left. \times \frac{1}{\omega_{cv}^2} \left(\frac{1}{\omega_{cv} - \omega} - \frac{4}{\omega_{cv} - 2\omega} \right) r_{vc}^a r_{cv}^b \Delta_{cv}^c - \frac{1}{2\omega_{cv}(\omega_{cv} - \omega)} r_{vc;a}^b r_{cv}^c \right] + (b \leftrightarrow c). \end{aligned} \quad (\text{E2})$$

The two contributions comes from interband and intraband scattering, respectively.

Since the diagonal part of r_{nm} is zero, for two-band systems, the contribution from interband scattering vanishes. We use the following identity for the generalized derivative:

$$(r_{nm}^b)_{,a} = \frac{r_{nm}^a \Delta_{mn}^b + r_{nm}^b \Delta_{mn}^a}{\omega_{nm}} + \frac{i}{\omega_{nm}} \sum_l (\omega_{lm} r_{nl}^a r_{lm}^b - \omega_{nl} r_{nl}^a r_{lm}^b) + \frac{w^{ab}}{i\omega_{nm}}. \quad (\text{E3})$$

Since we focus on a two-band system and since the diagonal parts of r_{nm} and ω_{nm} are zero, we can ignore the second term (the sum over all the other bands) in Eq. (E3).

We can write the two-photon and one-photon contributions individually for the symmetric case of σ^{abb} as follows:

$$\sigma_{1p,\text{SHG}}^{\text{abb}} = \frac{\omega e^3}{\hbar^2} \int [dk] \frac{f_{vc}}{\omega_{cv}^2 (\omega_{cv} - \omega)} \left(2r_{cv}^b r_{vc}^a \Delta_{cv}^b - |r_{cv}^b|^2 \Delta_{cv}^a + i w_{cv}^{ab} r_{vc}^b \right), \quad (\text{E4})$$

$$\sigma_{2p,\text{SHG}}^{\text{abb}} = \frac{2\omega e^3}{\hbar^2} \int [dk] f_{vc} \left(\frac{-8r_{vc}^a r_{cv}^b \Delta_{cv}^b}{\omega_{cv}^2 (\omega_{cv} - 2\omega)} - \frac{2i w_{cv}^{bb} r_{vc}^a}{\omega_{cv} (\omega_{cv} - 2\omega)} \right). \quad (\text{E5})$$

Models

In this section we investigate the singular behavior of the SHG in nodal line semimetals in the length gauge. The most singular behavior has been seen in the zzz direction for SHG; thus we only focus on this direction in this section.

By using the relation $i r_{nm}^i = \frac{v_{nm}}{\omega_{nm}}$ we can simplify the conductivity in the following way:

$$\sigma_{1p,\text{SHG}}^{\text{abb}} = \frac{\omega e^3}{\hbar^2} \int [dk] \frac{f_{vc}}{\omega_{cv}^3 (\omega_{cv} - \omega)} \left(\frac{|v_{cv}^z|^2 \Delta_{cv}^z}{\omega_{cv}} + w_{cv}^{zz} v_{vc}^z \right), \quad (\text{E6})$$

$$\sigma_{2p,\text{SHG}}^{\text{abb}} = \frac{2\omega e^3}{\hbar^2} \int [dk] f_{vc} \left(\frac{8v_{vc}^z v_{cv}^z \Delta_{cv}^z}{\omega_{cv}^4 (\omega_{cv} - 2\omega)} + \frac{2i w_{cv}^{zz} v_{vc}^z}{\omega_{cv}^2 (\omega_{cv} - 2\omega)} \right). \quad (\text{E7})$$

The structures of Eqs. (E6) and (E7) are closely related to the structures of Eqs. (C6)–(C9).

For a nodal line Hamiltonian [Eq. (16)] we can simplify the above equation as follows:

$$\sigma_{2p,\text{SHG}}^{\text{abb}} = \frac{2\omega e^3}{\hbar^2} \int [dk] \frac{e\tau}{\hbar} E_z \partial_{k_z} \epsilon \frac{\partial f_n^{(0)}(\epsilon)}{\partial \epsilon(k)} \frac{-4(\sqrt{k_x^2 + k_y^2} - k_0)^2 k_z v^2}{[(\sqrt{k_x^2 + k_y^2} - k_0)^2 + k_z^2]^2} \frac{1}{\omega_{cv}^3} R_\gamma(\omega_{cv} - 2\omega). \quad (\text{E8})$$

By using the variable change in Eq. (B4) we simplify the equation to find the behavior of the SHG

$$\sigma_{2p,\text{SHG}}^{\text{abb}} \approx \frac{-e^4 E_z v \tau}{2\hbar^3 \omega^2} \int_0^\infty dd \int_0^{2\pi} d\theta \int_0^{2\pi} d\phi (k_0 v + d \sin(\theta)) \sin(2\theta)^2 R_\gamma(2\omega - 2d) \delta(d - \mu), \quad (\text{E9})$$

in which

$$\sigma_{2p,\text{SHG}}^{\text{abb}} \approx \frac{e^4 E_z k_0 v^2 \tau}{\hbar^3 \omega^2} R_\gamma(2\omega - 2\mu) \quad (\text{E10})$$

has the same behavior as SHG in the velocity gauge.

- [1] R. Boyd, *Nonlinear Optics*, 3rd ed. (Academic, Amsterdam, 2008).
- [2] K. Takasan, T. Morimoto, J. Orenstein, and J. E. Moore, Current-induced second harmonic generation in inversion-symmetric Dirac and Weyl semimetals, *Phys. Rev. B* **104**, L161202 (2021).
- [3] W. Kraut and R. von Baltz, Anomalous bulk photovoltaic effect in ferroelectrics: A quadratic response theory, *Phys. Rev. B* **19**, 1548 (1979).
- [4] V. I. Belinicher and B. I. Sturman, The photogalvanic effect in media lacking a center of symmetry, *Sov. Phys.-Usp.* **23**, 199 (1980).
- [5] R. von Baltz and W. Kraut, Theory of the bulk photovoltaic effect in pure crystals, *Phys. Rev. B* **23**, 5590 (1981).
- [6] C. Aversa and J. E. Sipe, Nonlinear optical susceptibilities of semiconductors: Results with a length-gauge analysis, *Phys. Rev. B* **52**, 14636 (1995).
- [7] B. I. Sturman and V. M. Fridkin, *The Photovoltaic and Photorefractive Effects in Noncentrosymmetric Materials*, Ferroelectricity and Related Phenomena (Routledge, London, 1992), Vol. 8, p. 14176.
- [8] A. M. Cook, B. M. Fregoso, F. de Juan, S. Coh, and J. E. Moore, Design principles for shift current photovoltaics, *Nat. Commun.* **8**, 14176 (2017).
- [9] J. E. Sipe and A. I. Shkrebtii, Second-order optical response in semiconductors, *Phys. Rev. B* **61**, 5337 (2000).
- [10] J. B. Khurgin, Current induced second harmonic generation in semiconductors, *Appl. Phys. Lett.* **67**, 1113 (1995).
- [11] S. Wu, L. Mao, A. M. Jones, W. Yao, C. Zhang, and X. Xu, Quantum-enhanced tunable second-order optical nonlinearity in bilayer graphene, *Nano Lett.* **12**, 2032 (2012).
- [12] S. Patankar, L. Wu, B. Lu, M. Rai, J. D. Tran, T. Morimoto, D. E. Parker, A. G. Grushin, N. L. Nair, J. G. Analytis, J. E. Moore, J. Orenstein, and D. H. Torchinsky, Resonance-enhanced optical nonlinearity in the Weyl semimetal TaAs, *Phys. Rev. B* **98**, 165113 (2018).
- [13] C. H. Lee, H. H. Yap, T. Tai, G. Xu, X. Zhang, and J. Gong, Enhanced higher harmonic generation from nodal topology, *Phys. Rev. B* **102**, 035138 (2020).
- [14] A. de la Torre, S. Di Matteo, D. Hsieh, and M. R. Norman, Implications of second harmonic generation for hidden order in $\text{Sr}_2\text{CuO}_2\text{Cl}_2$, *Phys. Rev. B* **104**, 035138 (2021).
- [15] H. Chu, C. J. Roh, J. O. Island, C. Li, S. Lee, J. Chen, J.-G. Park, A. F. Young, J. S. Lee, and D. Hsieh, Linear Magnetoelectric Phase in Ultrathin MnPS_3 Probed by Optical Second Harmonic Generation, *Phys. Rev. Lett.* **124**, 027601 (2020).
- [16] B. M. Fregoso, Bulk photovoltaic effects in the presence of a static electric field, *Phys. Rev. B* **100**, 064301 (2019).
- [17] T. Morimoto and N. Nagaosa, Topological nature of nonlinear optical effects in solids, *Sci. Adv.* **2**, e1501524 (2016).
- [18] N. P. Armitage, E. J. Mele, and A. Vishwanath, Weyl and Dirac semimetals in three-dimensional solids, *Rev. Mod. Phys.* **90**, 015001 (2018).
- [19] F. de Juan, A. G. Grushin, T. Morimoto, and J. E. Moore, Quantized circular photogalvanic effect in Weyl semimetals, *Nat. Commun.* **8**, 15995 (2017).
- [20] C.-K. Chan, N. H. Lindner, G. Refael, and P. A. Lee, Photocurrents in Weyl semimetals, *Phys. Rev. B* **95**, 041104(R) (2017).
- [21] L. Wu, S. Patankar, T. Morimoto, N. L. Nair, E. Thewalt, A. Little, J. G. Analytis, J. E. Moore, and J. Orenstein, Giant anisotropic nonlinear optical response in transition metal monopnictide Weyl semimetals, *Nat. Phys.* **13**, 350 (2016).
- [22] G. B. Osterhoudt, L. K. Diebel, M. J. Gray, X. Yang, J. Stanco, X. Huang, B. Shen, N. Ni, P. J. W. Moll, Y. Ran, and K. S. Burch, Colossal mid-infrared bulk photovoltaic effect in a type-I Weyl semimetal, *Nat. Mater.* **18**, 471 (2019).
- [23] V. D. Esin, A. V. Timonina, N. N. Kolesnikov, and E. V. Deviatov, Second-harmonic voltage response for the magnetic Weyl semimetal $\text{Co}_3\text{Sn}_2\text{S}_2$, *JETP Lett.* **111**, 685 (2020).
- [24] Y. Gao, F. Zhang, and W. Zhang, Second-order nonlinear Hall effect in Weyl semimetals, *Phys. Rev. B* **102**, 245116 (2020).
- [25] S. Nandy, C. Zeng, and S. Tewari, Chiral anomaly induced nonlinear Hall effect in semimetals with multiple Weyl points, *Phys. Rev. B* **104**, 205124 (2021).
- [26] J. E. Moore and J. Orenstein, Confinement-Induced Berry Phase and Helicity-Dependent Photocurrents, *Phys. Rev. Lett.* **105**, 026805 (2010).
- [27] E. Deyo, L. E. Golub, E. L. Ivchenko, and B. Spivak, Semiclassical theory of the photogalvanic effect in non-centrosymmetric systems, [arXiv:0904.1917](https://arxiv.org/abs/0904.1917) [cond-mat.mes-hall].
- [28] I. Sodemann and L. Fu, Quantum Nonlinear Hall Effect Induced by Berry Curvature Dipole in Time-Reversal Invariant Materials, *Phys. Rev. Lett.* **115**, 216806 (2015).
- [29] S. M. Young and A. M. Rappe, First Principles Calculation of the Shift Current Photovoltaic Effect in Ferroelectrics, *Phys. Rev. Lett.* **109**, 116601 (2012).
- [30] X. Yang, K. Burch, and Y. Ran, Divergent bulk photovoltaic effect in Weyl semimetals, [arXiv:1712.09363](https://arxiv.org/abs/1712.09363) [cond-mat.mes-hall].
- [31] N. Sirica, R. I. Tobey, L. X. Zhao, G. F. Chen, B. Xu, R. Yang, B. Shen, D. A. Yarotski, P. Bowlan, S. A. Trugman, J.-X. Zhu, Y. M. Dai, A. K. Azad, N. Ni, X. G. Qiu, A. J. Taylor, and R. P. Prasankumar, Tracking Ultrafast Photocurrents in the Weyl Semimetal TaAs Using THz Emission Spectroscopy, *Phys. Rev. Lett.* **122**, 197401 (2019).
- [32] C. Fang, Y. Chen, H.-Y. Kee, and L. Fu, Topological nodal line semimetals with and without spin-orbital coupling, *Phys. Rev. B* **92**, 081201(R) (2015).
- [33] C. Fang, H. Weng, X. Dai, and Z. Fang, Topological nodal line semimetals, *Chin. Phys. B* **25**, 117106 (2016).
- [34] J.-W. Rhim and Y. B. Kim, Landau level quantization and almost flat modes in three-dimensional semimetals with nodal ring spectra, *Phys. Rev. B* **92**, 045126 (2015).
- [35] G. Xu, H. Weng, Z. Wang, X. Dai, and Z. Fang, Chern Semimetal and the Quantized Anomalous Hall Effect in HgCr_2Se_4 , *Phys. Rev. Lett.* **107**, 186806 (2011).
- [36] R. Yu, H. Weng, Z. Fang, X. Dai, and X. Hu, Topological Node-Line Semimetal and Dirac Semimetal State in Antiperovskite Cu_3PdN , *Phys. Rev. Lett.* **115**, 036807 (2015).
- [37] Y. Kim, B. J. Wieder, C. L. Kane, and A. M. Rappe, Dirac Line Nodes in Inversion-Symmetric Crystals, *Phys. Rev. Lett.* **115**, 036806 (2015).
- [38] Y.-H. Chan, C.-K. Chiu, M. Y. Chou, and A. P. Schnyder, Ca_3P_2 and other topological semimetals with line nodes and drumhead surface states, *Phys. Rev. B* **93**, 205132 (2016).
- [39] L. M. Schoop, M. N. Ali, C. Straßer, A. Topp, A. Varykhalov, D. Marchenko, V. Duppel, S. S. P. Parkin, B. V. Lotsch, and C. R. Ast, Dirac cone protected by non-symmorphic symmetry and three-dimensional Dirac line node in ZrSiS , *Nat. Commun.* **7**, 11696 (2016).

- [40] Y. Chen, Y.-M. Lu, and H.-Y. Kee, Topological crystalline metal in orthorhombic perovskite iridates, *Nat. Commun.* **6**, 6593 (2015).
- [41] T. Tai and C. H. Lee, Anisotropic nonlinear optical response of nodal-loop materials, *Phys. Rev. B* **103**, 195125 (2021).
- [42] C. H. Lee, X. Zhang, and B. Guan, Negative differential resistance and characteristic nonlinear electromagnetic response of a topological insulator, *Sci. Rep.* **5**, 18008 (2015).
- [43] A. Martín-Ruiz and A. Cortijo, Parity anomaly in the nonlinear response of nodal-line semimetals, *Phys. Rev. B* **98**, 155125 (2018).
- [44] D. Sinha and A. Taraphder, Giant nonlinear response due to unconventional magneto-oscillations in nodal-line semimetals, *Phys. Rev. B* **104**, 245141 (2021).
- [45] D. J. Moss, E. Ghahramani, J. E. Sipe, and H. M. van Driel, Band-structure calculation of dispersion and anisotropy in $\chi \rightarrow^{(3)}$ for third-harmonic generation in Si, Ge, and GaAs, *Phys. Rev. B* **41**, 1542 (1990).
- [46] J.-W. Rhim and Y. B. Kim, Anisotropic density fluctuations, plasmons, and Friedel oscillations in nodal line semimetal, *New J. Phys.* **18**, 043010 (2016).
- [47] H. Yang, R. Moessner, and L.-K. Lim, Quantum oscillations in nodal line systems, *Phys. Rev. B* **97**, 165118 (2018).
- [48] Y. Huh, E.-G. Moon, and Y. B. Kim, Long-range Coulomb interaction in nodal-ring semimetals, *Phys. Rev. B* **93**, 035138 (2016).
- [49] W. B. Rui, Y. X. Zhao, and A. P. Schnyder, Topological transport in Dirac nodal-line semimetals, *Phys. Rev. B* **97**, 161113(R) (2018).
- [50] T. Shang, S. K. Ghosh, M. Smidman, D. J. Gawryluk, C. Baines, A. Wang, W. Xie, Y. Chen, M. O. Ajeesh, M. Nicklas, E. Pomjakushina, M. Medarde, M. Shi, J. F. Annett, H. Yuan, J. Quintanilla, and T. Shiroka, Spin-triplet superconductivity in Weyl nodal-line semimetals, *npj Quantum Mater.* **7**, 35 (2022).
- [51] S. N. Rashkeev and W. R. L. Lambrecht, Second-harmonic generation of I-III-VI₂ chalcopyrite semiconductors: Effects of chemical substitutions, *Phys. Rev. B* **63**, 165212 (2001).
- [52] J. L. P. Hughes and J. E. Sipe, Calculation of second-order optical response in semiconductors, *Phys. Rev. B* **53**, 10751 (1996).